

## Chapter 7. Trends in IMPROVE Reconstructed Light Extinction Coefficients

Temporal trends were calculated for speciated aerosol extinction coefficients, including extinction due to ammonium sulfate ( $b_{\text{ext\_AS}}$ ), ammonium nitrate ( $b_{\text{ext\_AN}}$ ), particulate organic matter ( $b_{\text{ext\_POM}}$ ), elemental carbon ( $b_{\text{ext\_EC}}$ ), fine dust ( $b_{\text{ext\_FD}}$ ), coarse mass ( $b_{\text{ext\_CM}}$ ), aerosol extinction ( $b_{\text{ext\_aer}}$ ), total extinction (aerosol and Rayleigh,  $b_{\text{ext\_tot}}$ ), and deciview (dv). Trends in sea salt extinction ( $b_{\text{ext\_SS}}$ ) were not calculated because of negative biases in chloride concentrations from 2007 to 2011 (Zhang, 2019). For all of the parameters, long-term (30 years, 1990–2019) and short-term (20 years, 2000–2019) trends were computed. Short-term trends take advantage of the network expansion in 2000 that resulted in greater site coverage across the country. Trend analyses were not performed for Chemical Speciation Network data because of the many changes starting in 2016 that resulted in some shifts to the data that require further evaluation before trends can be accurately interpreted (see Appendix 1.2).

Site-specific trends were computed for the same eight parameters as mass trends: 10<sup>th</sup>, 50<sup>th</sup>, and 90<sup>th</sup> percentiles and winter (DJF), spring (MAM), summer (JJA), fall (SON), and annual means. Winter means include the December data from the previous year. Fifty percent of daily data was required for a valid seasonal mean, and annual means were calculated from four valid seasonal means. Annual percentiles were calculated for 60% of valid daily data. Sites for long- and short-term trends required 70% of the years to be valid. A Theil regression was performed with the  $b_{\text{ext}}$  data as the dependent variable and the year as the independent variable. An advantage to the Theil regression is that heavy influence by outliers on the regression results is avoided (Theil, 1950). Kendall tau statistics were used to determine the statistical significance, assuming the slope was statistically significant at 5% ( $p \leq 0.05$ ), meaning that there was a 95% chance that the slope was not due to random chance. Trends (% yr<sup>-1</sup>) were calculated by dividing the slope by the median  $b_{\text{ext}}$  value over the time period of the trend, multiplied by 100%. Reporting trends instead of slopes normalizes the range in  $b_{\text{ext}}$  values that occurred across the United States. However, trends can be large (>100%) when median  $b_{\text{ext}}$  values are very low (e.g., 10<sup>th</sup> percentile).

Short-term regional mean trends were calculated for ten regions of the United States. Sites were grouped by their state into the following regions: Northeast, Southeast, Midsouth, Central, Southwest, Northwest, California, Alaska, Hawaii, Virgin Islands (See Table 6.0 and Figure 6.0), and the continental United States (CONUS). The Virgin Islands region included one site. Only sites that met the 70% valid data trend requirement were included in the regional trend calculation. Although some names are the same, these regions are broader and do not correspond to the regions shown in Chapters 3 and 5. The regions were qualitatively determined only as a means for summarizing trends. Regional mean trends were computed by aggregating site-specific seasonal mean  $b_{\text{ext}}$  (or percentiles) for a given region and year and then performing a Theil regression on regional mean  $b_{\text{ext}}$ . Regional mean trends were calculated for seasonal and annual means and for the 10<sup>th</sup>, 50<sup>th</sup>, and 90<sup>th</sup> percentiles. Annual mean trends can be driven by trends during specific seasons, and different percentiles may correspond to different trends, so regional mean trends were categorized by these aggregations to provide further insight into the temporal behavior of major aerosol extinction components.

Trend results were interpolated to provide isopleths to guide the eye (Isaaks and Mohan Srivastava, 1989). Site-specific positive trends were denoted with an upward-pointing triangle and contoured with warm colors. Negative trends were shown with downward-pointing triangles and contoured with cold colors. Statistically significant trends ( $p \leq 0.05$ ) were denoted with filled triangles. Scales were kept similar for all parameters so that trends can be compared. Long-term trend maps suffer from lower site densities, and therefore interpolations in regions without long-term sites (such as the central United States) should be viewed only as a spatial transition.

Speciated  $b_{\text{ext}}$  trends were similar to mass trends, especially for nonhygroscopic species. Differences in trends may arise depending on treatment of negative extinction values, which can occur for (very small) negative mass concentrations. While negative mass values reflect uncertainties in the measurements, negative  $b_{\text{ext}}$  values are unphysical and were set to zero.

## 7.1 AMMONIUM SULFATE LIGHT EXTINCTION COEFFICIENT TRENDS

Long- and short-term annual mean  $b_{\text{ext\_AS}}$  trends are shown in Figures 7.1.1a and 7.1.1b, respectively. All of the 55 valid sites met long-term completeness criteria, and all were statistically significant. Reductions of  $b_{\text{ext\_AS}}$  were strongest at sites in the eastern United States, in the Appalachian Mountains and Ohio River valley areas, where sulfur dioxide emissions have decreased dramatically and have led to improvements in visibility (Hand et al., 2014; Hand et al., 2020). Long-term annual mean  $b_{\text{ext\_AS}}$  trends ranged from  $-7.91\% \text{ yr}^{-1}$  ( $p < 0.001$ ) at Shining Rock Wilderness Area (WA), North Carolina (SHRO1), to  $-0.97\% \text{ yr}^{-1}$  ( $p = 0.02$ ) at Lassen Volcanic National Park (NP), California (LAVO1). Less progress occurred for sites in California, Nevada, and Idaho, as well as southwest Texas. Trends at these sites were between  $-1$  and  $-2\% \text{ yr}^{-1}$ . The West has historically had lower sulfur dioxide emissions than the eastern United States (Hand et al., 2012; Hand et al., 2020), and therefore the reduction of those regulated emissions has had less of an impact on already-low extinction values.

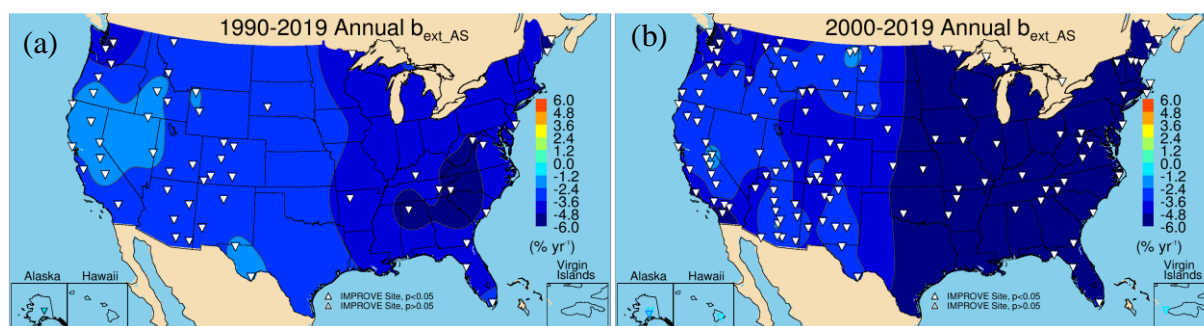


**Figure 7.1.1. Annual mean ammonium sulfate  $b_{\text{ext}}$  ( $b_{\text{ext\_AS}}$ ) trends ( $\% \text{ yr}^{-1}$ ) for (a) long-term (1990–2019) and (b) short-term (2000–2019) periods. Filled triangles correspond to statistically significant trends ( $p \leq 0.05$ ).**

Trends in short-term annual mean  $b_{\text{ext\_AS}}$  were negative for all valid sites shown in Figure 7.1.1b. Out of the 135 valid sites, 130 were statistically significant and ranged from  $-11.55\% \text{ yr}^{-1}$  ( $p < 0.001$ ) at (FRRE1) to  $1.93\% \text{ yr}^{-1}$  ( $p = 0.003$ ) at (HOOV1). Insignificant trends occurred at sites in Hawaii, Alaska, and the Virgin Islands. A strong spatial gradient in annual mean trends existed between the eastern and western United States, with stronger rates of change for sites in the East. Sites east of  $-100^\circ$  nearly all had  $b_{\text{ext\_AS}}$  decrease at rates greater than  $-4\% \text{ yr}^{-1}$ , and in the Appalachia and Ohio River valley areas, trends were around  $-7\% \text{ yr}^{-1}$  to  $-10\% \text{ yr}^{-1}$ ,

corresponding to a 140–200% decrease over the past two decades. Trends in the western United States were about  $-2\% \text{ yr}^{-1}$  to  $-4\% \text{ yr}^{-1}$ .

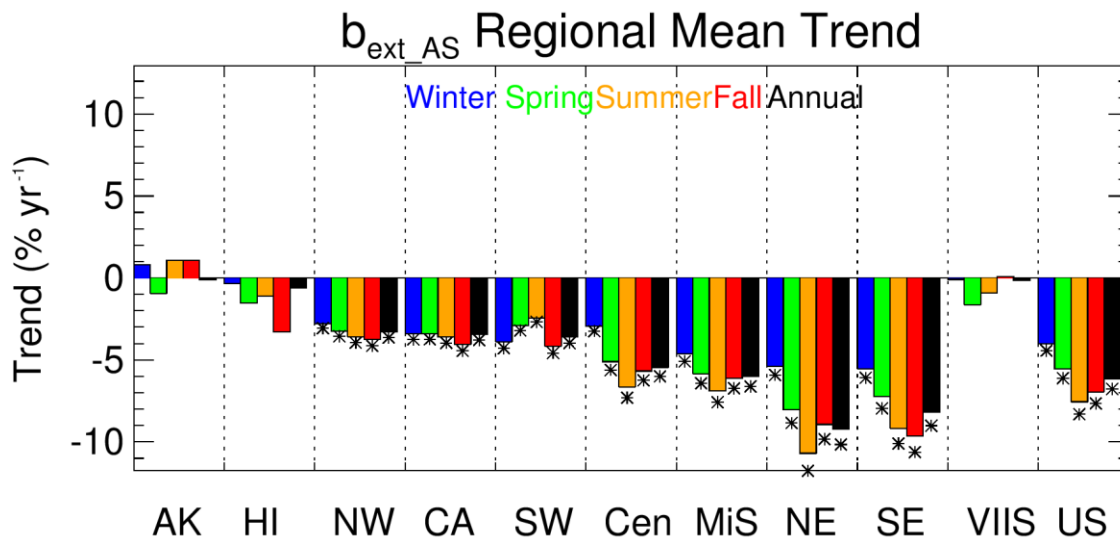


**Figure 7.1.2.** Short-term (2000–2019) regional seasonal mean ammonium sulfate  $b_{\text{ext}}$  ( $b_{\text{ext\_AS}}$ ) trends ( $\% \text{ yr}^{-1}$ ) for major U.S. regions for winter, spring, summer, fall, and annual means. Regions are arranged from western to eastern United States (AK = Alaska, HI = Hawaii, NW = Northwest, CA = California, SW = Southwest, Cen = Central, MiS = Midsouth, NE = Northeast, SE = Southeast, VIIS = Virgin Islands, and US = all sites). Statistically significant trends ( $p \leq 0.05$ ) are denoted with “\*”.

Regional seasonal mean  $b_{\text{ext\_AS}}$  trends are presented in Figure 7.1.2 and were similar to regional mean mass trends. The largest reductions in seasonal mean  $b_{\text{ext\_AS}}$  occurred for sites in the Northeast region ( $-10.70\% \text{ yr}^{-1}$  in summer), followed by the Southeast region ( $-9.66\% \text{ yr}^{-1}$  in fall). The least negative regional mean trends in the East occurred during winter. Trends were lower at regions in the western United States ( $-3\% \text{ yr}^{-1}$  to  $-4\% \text{ yr}^{-1}$ ), and the range in seasonal mean trends were lower. The exception to this is in the Southwest region, where summer trends were lower relative to other seasons. Overall, across the United States, negative  $b_{\text{ext\_AS}}$  trends were strongest during summer and fall. Seasonal regional mean trends at sites in Alaska, Hawaii, and the Virgin Islands were all relatively flat and insignificant.

Long-term 10<sup>th</sup> and 90<sup>th</sup> percentile  $b_{\text{ext\_AS}}$  trends are shown in Figure 7.1.3a and 7.1.3b, respectively. The spatial variability for the 10<sup>th</sup> and 90<sup>th</sup> percentile trends were similar, with larger reductions at sites in the eastern United States. The 10<sup>th</sup> percentile trends ranged from  $-5.74\% \text{ yr}^{-1}$  ( $p < 0.001$ ) at Shining Rock WA, North Carolina (SHRO1), to  $-1.34\% \text{ yr}^{-1}$  ( $p = 0.008$ ) at Jarbidge WA, Nevada (JARB1), and 54 out of 57 sites had statistically significant trends. Insignificant trends occurred at Hawaii Volcanoes NP, Hawaii (HAVO1), Lassen Volcanic NP, California (LAVO1), and Three Sisters WA, Oregon (THSI1). Trends in the 10<sup>th</sup> percentile  $b_{\text{ext\_AS}}$  at sites in California were weaker ( $\sim -2\% \text{ yr}^{-1}$ ) than at other sites in the United States.

Trend values did not differ greatly for the long-term 90<sup>th</sup> percentile  $b_{\text{ext\_AS}}$  (Figure 7.1.3b) compared to the 10<sup>th</sup> percentile  $b_{\text{ext\_AS}}$  trends, and 56 out of 57 sites had statistically significant

trends. The largest negative trend occurred at Shining Rock WA, North Carolina (SHRO1,  $-7.20\% \text{ yr}^{-1}$ ,  $p < 0.001$ ), compared to the lowest negative trend at Big Bend NP, Texas (BIBE1,  $-1.02\% \text{ yr}^{-1}$ ,  $p = 0.012$ ).

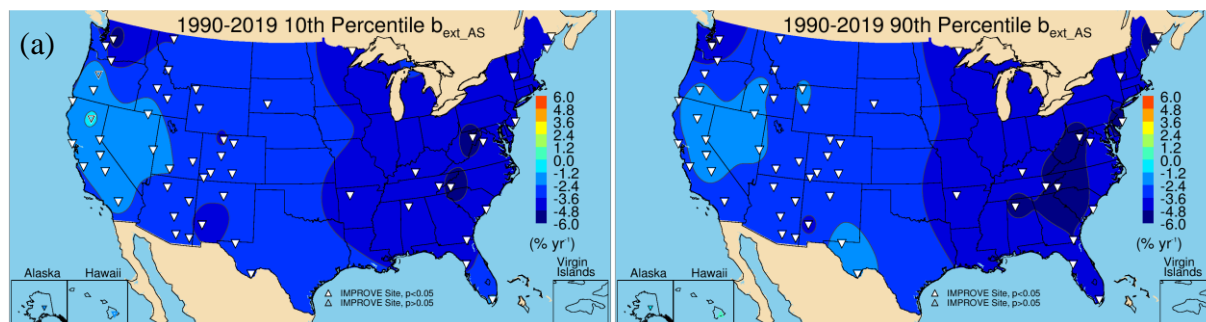


**Figure 7.1.3. IMPROVE long-term (1990–2019) trends ( $\% \text{ yr}^{-1}$ ) in (a) 10<sup>th</sup> percentile ammonium sulfate  $b_{\text{ext\_AS}}$  and (b) 90<sup>th</sup> percentile  $b_{\text{ext\_AS}}$ . Filled triangles correspond to statistically significant trends ( $p \leq 0.05$ ).**

Short-term trends in the 10<sup>th</sup> and 90<sup>th</sup>  $b_{\text{ext\_AS}}$  are shown in Figure 7.1.4a and 7.1.4b, respectively. Large-scale spatial variability in trends was similar for both percentiles, with greater reductions in  $b_{\text{ext\_AS}}$  at sites in the eastern United States. Differences in the spatial patterns occurred at sites in the central United States where the 90<sup>th</sup> percentile trends were stronger (e.g., Kansas and Oklahoma and in southern California). At sites in the northwestern United States, 10<sup>th</sup> percentile trends were stronger. For 138 valid sites with 10<sup>th</sup> percentile trends, 126 were statistically significant, compared to 132 for 90<sup>th</sup> percentile trends. The largest reductions in 10<sup>th</sup> percentile  $b_{\text{ext\_AS}}$  occurred at Cohutta, Georgia (COHU1,  $-8.32\% \text{ yr}^{-1}$ ,  $p < 0.001$ ), compared to lowest reduction at Crater Lake NP, California (CRLA1,  $-1.78\% \text{ yr}^{-1}$ ,  $p = 0.04$ ). The largest reduction in the 90<sup>th</sup> percentile  $b_{\text{ext\_AS}}$  also occurred at Cohutta, Georgia (COHU1,  $-14.38\% \text{ yr}^{-1}$ ,  $p < 0.001$ ), compared to the lowest reduction at Kaiser, California (KAIS1,  $-1.45\% \text{ yr}^{-1}$ ,  $p = 0.009$ ). For both the 10<sup>th</sup> and 90<sup>th</sup> percentiles, trends were insignificant at sites in Alaska, Hawaii, and the Virgin Islands.

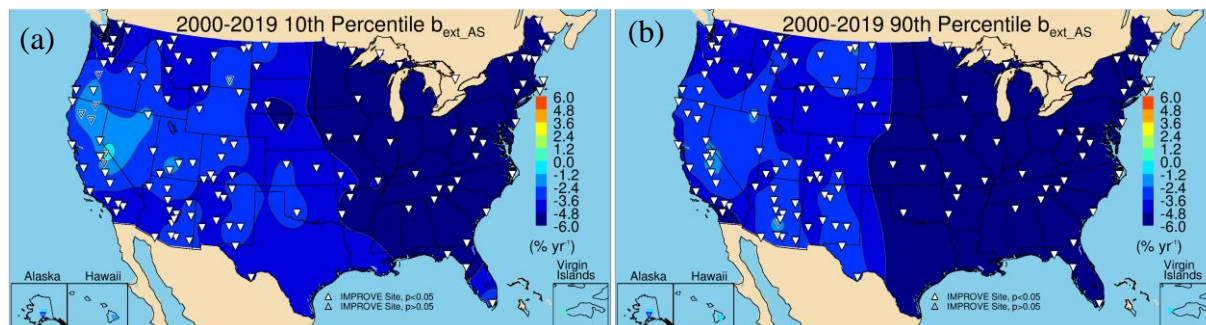


**Figure 7.1.4. IMPROVE short-term (2000–2019) trends ( $\% \text{ yr}^{-1}$ ) in (a) 10<sup>th</sup> percentile ammonium sulfate  $b_{\text{ext}}$  and (b) 90<sup>th</sup> percentile  $b_{\text{ext\_AS}}$ . Filled triangles correspond to statistically significant trends ( $p \leq 0.05$ ).**

Comparisons of regional mean percentile trends are shown in Figure 7.1.5. For most regions in the western United States, the 10<sup>th</sup>, 50<sup>th</sup>, and 90<sup>th</sup> percentile trends were similar, with the Northwest region having slightly greater reductions in the 10<sup>th</sup> percentile  $b_{\text{ext\_AS}}$  as suggested in Figures 7.1.4a and 7.1.4b. However, for eastern regions, the regional mean 90<sup>th</sup> percentile trends decreased at a much greater rate than the other percentile trends. The 90<sup>th</sup> percentile trend

in the Northeast region was  $-11.25\% \text{ yr}^{-1}$  compared to the 10<sup>th</sup> percentile trend of  $-6.37\% \text{ yr}^{-1}$ . The Southeast region had similar differences in the 90<sup>th</sup> and 10<sup>th</sup> percentile trends ( $-9.83\% \text{ yr}^{-1}$  compared to  $-5.44\% \text{ yr}^{-1}$ ,  $p < 0.001$ , respectively). These trends are consistent with the strongest seasonal mean trends occurring in summer, when the highest  $b_{\text{ext\_AS}}$  typically occurred.

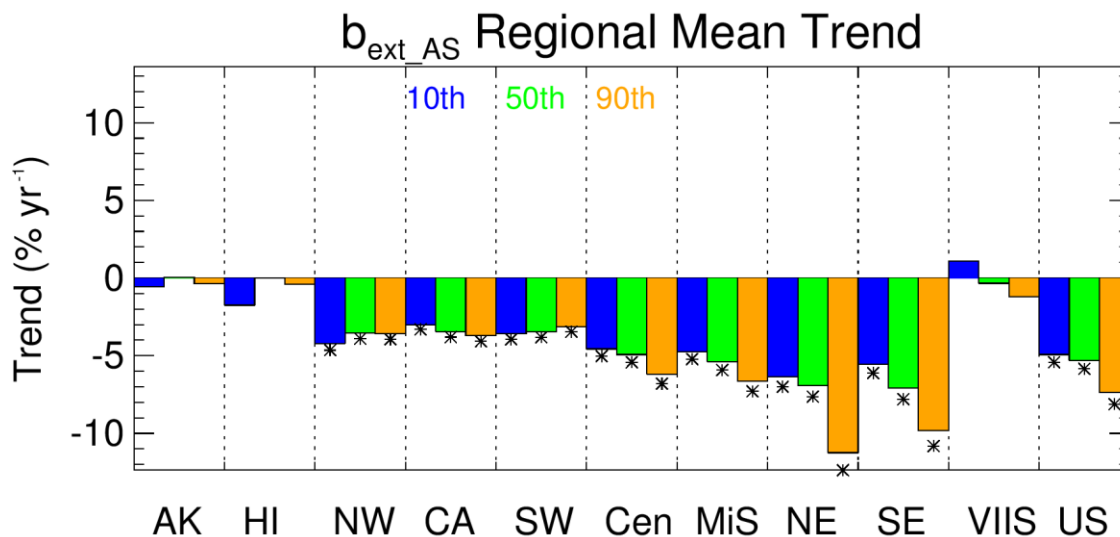


**Figure 7.1.5.** Short-term (2000–2019) regional mean trends ( $\% \text{ yr}^{-1}$ ) in 10<sup>th</sup>, 50<sup>th</sup>, and 90<sup>th</sup> percentile ammonium sulfate  $b_{\text{ext}}$  ( $b_{\text{ext\_AS}}$ ). Regions are arranged from western to eastern United States (AK = Alaska, HI = Hawaii, NW = Northwest, CA = California, SW = Southwest, Cen = Central, MiS = Midsouth, NE = Northeast, SE = Southeast, VIIS = Virgin Islands, and US = all sites). Statistically significant trends ( $p \leq 0.05$ ) are denoted with “\*”.

## 7.2 AMMONIUM NITRATE LIGHT EXTINCTION COEFFICIENT TRENDS

Long-term annual mean  $b_{\text{ext\_AN}}$  trends are shown in Figure 7.2.1a. Of the 42 valid trend sites, 36 had statistically significant trends. The largest reductions ( $\sim -3\% \text{ yr}^{-1}$ ) in the annual mean  $b_{\text{ext\_AN}}$  occurred at sites in southern California, with the largest negative trend at San Geronio WA, California (SAGO1,  $-7.75\% \text{ yr}^{-1}$ ,  $p < 0.001$ ). Strong reductions in  $b_{\text{ext\_AN}}$  at sites in California are associated with reduced nitrogen dioxide emissions from vehicles (Russell et al., 2012; Tong et al., 2015). Insignificant trends occurred at sites in Colorado, Texas, and New Mexico and were associated with nearly flat reductions. The lowest statistically significant trend occurred at Bridger WA, Wyoming (BRID1,  $-0.94\% \text{ yr}^{-1}$ ,  $p = 0.03$ ). Trends at sites in the eastern United States were about  $-1\% \text{ yr}^{-1}$  to  $-2\% \text{ yr}^{-1}$ .

Short-term annual mean  $b_{\text{ext\_AN}}$  trends also showed strong reductions at sites in southern California (Figure 7.2.1b). The strongest reduction for short-term trends occurred at Joshua Tree NP, California (JOSH1,  $-8.92\% \text{ yr}^{-1}$ ,  $p < 0.001$ ). Of the 134 valid trends, 110 were statistically significant. Insignificant trends at sites in the northern Great Plains ( $-1\% \text{ yr}^{-1}$  to  $-2\% \text{ yr}^{-1}$ ) were likely associated with oil and gas development in the region (Gebhart et al., 2018). The lowest statistically significant annual mean  $b_{\text{ext\_AN}}$  trend occurred at Medicine Lake, Montana (MELA1,  $-0.89\% \text{ yr}^{-1}$ ,  $p = 0.04$ ).

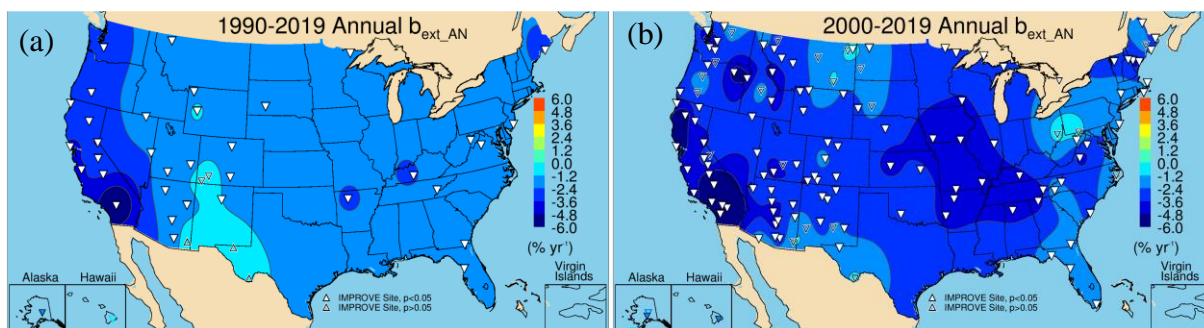


**Figure 7.2.1. Annual mean ammonium nitrate  $b_{ext\_AN}$  trends ( $\% \text{ yr}^{-1}$ ) for (a) long-term (1990–2019) and (b) short-term (2000–2019) periods. Filled triangles correspond to statistically significant trends ( $p \leq 0.05$ ).**

Comparisons of short-term regional seasonal mean  $b_{ext\_AN}$  trends are shown in Figure 7.2.2. The strongest reductions occurred in the California region, especially in the spring ( $-6.97\% \text{ yr}^{-1}$ ) and fall ( $-7.10\% \text{ yr}^{-1}$ ). Most regions had the strongest reductions during winter and least reductions in summer, with a large seasonal range. The exception was in the Northeast region where trends for all seasons were similar ( $\sim -2\% \text{ yr}^{-1}$  to  $-3\% \text{ yr}^{-1}$ ). This range in seasonal mean trends indicates potentially different sources and atmospheric processes controlling  $b_{ext\_AN}$  in these regions.

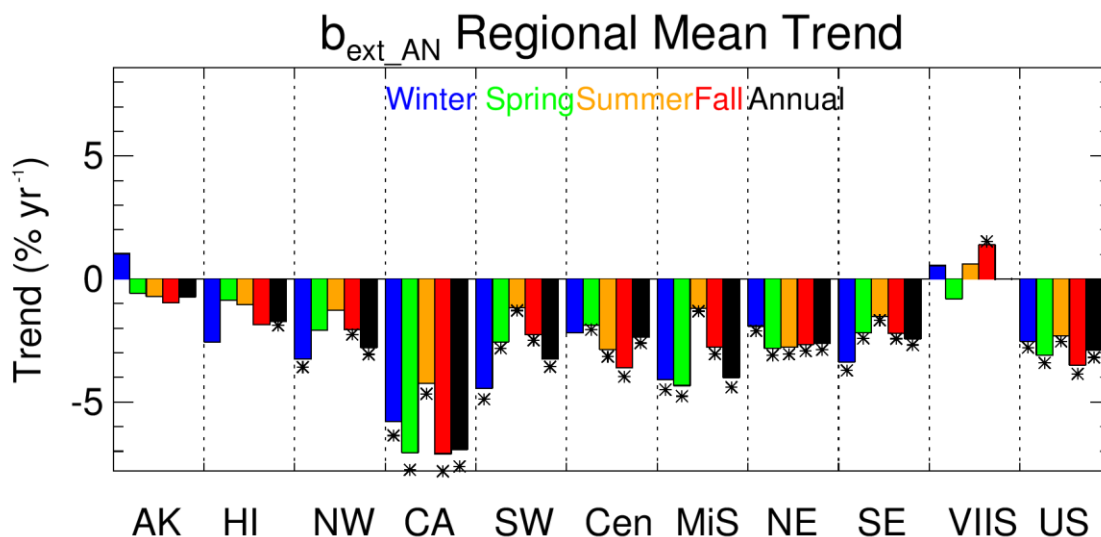


**Figure 7.2.2. Short-term (2000–2019) regional seasonal mean ammonium nitrate  $b_{ext}$  ( $b_{ext\_AN}$ ) trends ( $\% \text{ yr}^{-1}$ ) for major U.S. regions for winter, spring, summer, fall, and annual means. Regions are arranged from western to eastern United States (AK = Alaska, HI = Hawaii, NW = Northwest, CA = California, SW = Southwest, Cen = Central, MiS = Midsouth, NE = Northeast, SE = Southeast, VIIS = Virgin Islands, and US = all sites). Statistically significant trends ( $p \leq 0.05$ ) are denoted with “\*”.**

Long-term trends in the 10<sup>th</sup> and 90<sup>th</sup> percentile  $b_{ext\_AN}$  are shown in Figure 7.2.3a and 7.2.3b, respectively. Of the 45 valid 10<sup>th</sup> percentile trends, only 26 of them were statistically significant, and these occurred mainly at sites in California and the eastern United States. The strongest reduction in the 10<sup>th</sup> percentile  $b_{ext\_AN}$  occurred at San Gorgonio WA, California (SAGO1,  $-6.25\% \text{ yr}^{-1}$ ,  $p < 0.001$ ), compared to  $-0.88\% \text{ yr}^{-1}$  ( $p = 0.03$ ) at Weminuche WA,

Colorado (WEM11). Flat and insignificant trends occurred at sites located in the southwestern United States and the Intermountain West.

The spatial patterns in the long-term 90<sup>th</sup> percentile trends were similar to the 10<sup>th</sup> percentile trends, with the strongest reductions at sites in California and weak and insignificant trends at sites in the Southwest (Figure 7.2.3b). Trends ranged from  $-5.96\% \text{ yr}^{-1}$  ( $p < 0.001$ ) at San Gorgonio WA (SAGO1), to  $-0.88\% \text{ yr}^{-1}$  ( $p = 0.05$ ) at Jarbidge WA, Nevada (JARB1). However, more sites met statistical significance limits (32 out of 45) for 90<sup>th</sup> percentile trends. Some long-term 90<sup>th</sup> percentile trends in the eastern United States were weaker relative to the 10<sup>th</sup> percentile trends, but sites in the Intermountain West had stronger and statistically significant 90<sup>th</sup> percentile trends.

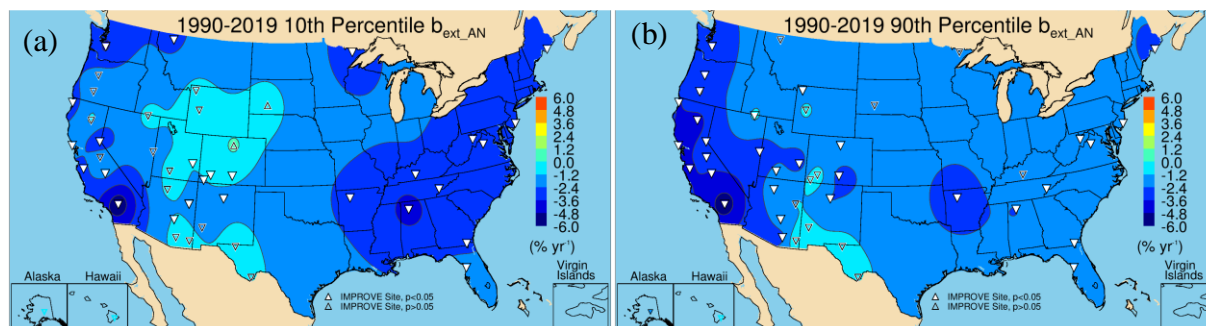


**Figure 7.2.3. IMPROVE long-term (1990–2019) trends ( $\% \text{ yr}^{-1}$ ) in (a) 10<sup>th</sup> percentile ammonium nitrate  $b_{\text{ext\_AN}}$  and (b) 90<sup>th</sup> percentile  $b_{\text{ext\_AN}}$ . Filled triangles correspond to statistically significant trends ( $p \leq 0.05$ ).**

The strongest reductions in short-term 10<sup>th</sup> percentile  $b_{\text{ext\_AN}}$  trends also occurred at San Gorgonio WA, California (SAGO1,  $-8.58\% \text{ yr}^{-1}$ ,  $p < 0.001$ ) (Figure 7.2.4a). Several sites in the eastern United States also experienced strong reductions in the 10<sup>th</sup> percentile  $b_{\text{ext\_AN}}$  ( $-5\% \text{ yr}^{-1}$  to  $-6\% \text{ yr}^{-1}$ ). Insignificant trends occurred at 81 of 138 valid sites. Positive but insignificant trends occurred at sites in the northern Great Plains, where oil and gas development has influenced  $b_{\text{ext\_AN}}$ . Other insignificant and flat trends occurred at sites in Colorado, Nebraska, South Dakota, Oregon, and Texas. The weakest significant trend occurred at Thunder Basin, Wyoming (THBA1,  $-1.09\% \text{ yr}^{-1}$ ,  $p = 0.04$ ).

The spatial patterns in the short-term 10<sup>th</sup> and 90<sup>th</sup> percentile trends (Figure 7.2.4b) were similar, with the strongest trends at sites in southern California and at sites in the Appalachian Mountains. Out of 138 valid 90<sup>th</sup> percentile trends, 101 met statistical significance requirements. Most of the insignificant trends also occurred at sites in the northern Great Plains area and near Maryland and Ohio (Frostburg Reservoir, Maryland, FRRE1, and Quaker City, Ohio, QUC11, respectively). The short-term 90<sup>th</sup> percentile trends ranged from  $-9.68\% \text{ yr}^{-1}$  ( $p = 0.011$ ) at Hells Canyon, Oregon (HECA1), to  $-1.43\% \text{ yr}^{-1}$  ( $p = 0.04$ ) at Hawaii Volcanoes NP, Hawaii (HAVO1).

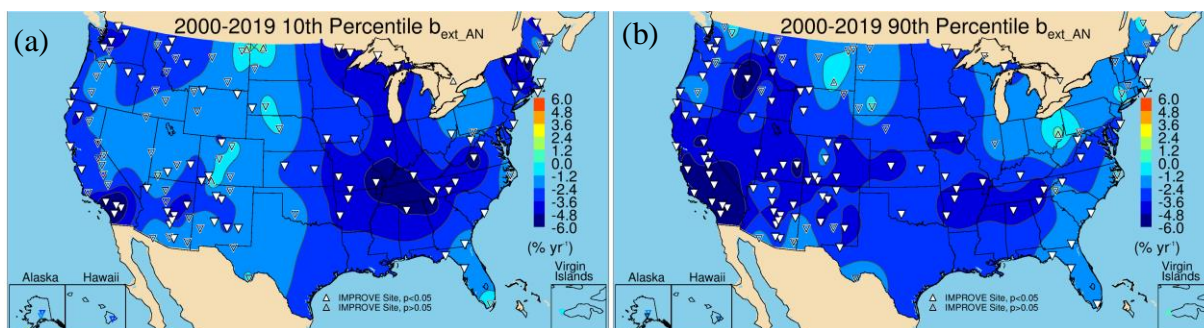


**Figure 7.2.4. IMPROVE short-term (2000–2019) trends (% yr<sup>-1</sup>) in (a) 10<sup>th</sup> percentile ammonium nitrate  $b_{ext}$  ( $b_{ext\_AN}$ ) and (b) 90<sup>th</sup> percentile  $b_{ext\_AN}$ . Filled triangles correspond to statistically significant trends ( $p \leq 0.05$ ).**

A summary of the regional mean 10<sup>th</sup>, 50<sup>th</sup>, and 90<sup>th</sup> percentile  $b_{ext\_AN}$  trends is shown in Figure 7.2.5. The strongest trends occurred in the California region, with the 90<sup>th</sup> percentile trends being the greatest (-6.77% yr<sup>-1</sup>,  $p < 0.001$ ). For all of the regions except the Central and Northeast regions, the 90<sup>th</sup> percentile trends were strongest. In the Central and Northeast regions, the 90<sup>th</sup> percentile trends were the weakest, and the 10<sup>th</sup> percentile trends were the strongest.

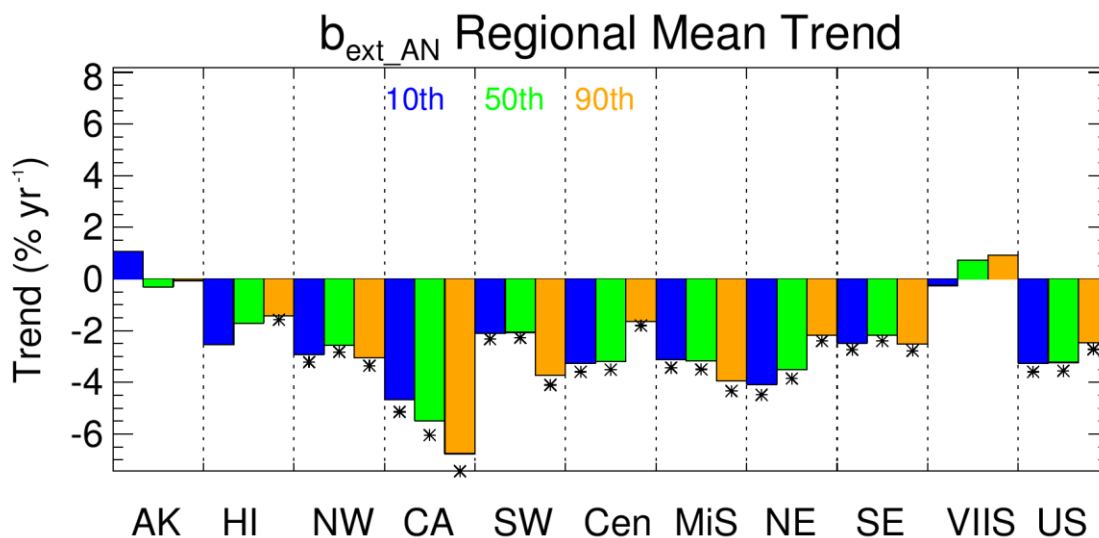


**Figure 7.2.5. Short-term (2000–2019) regional mean trends (% yr<sup>-1</sup>) in 10<sup>th</sup>, 50<sup>th</sup>, and 90<sup>th</sup> percentile ammonium nitrate  $b_{ext}$  ( $b_{ext\_AN}$ ). Regions are arranged from western to eastern United States (AK = Alaska, HI = Hawaii, NW = Northwest, CA = California, SW = Southwest, Cen = Central, MiS = MidSouth, NE = Northeast, SE = Southeast, VIIS = Virgin Islands, and US = all sites). Statistically significant trends ( $p \leq 0.05$ ) are denoted with “\*”.**

### 7.3 PARTICULATE ORGANIC MATTER LIGHT EXTINCTION COEFFICIENT TRENDS

Annual mean  $b_{ext\_POM}$  trends for long-term sites are shown in Figure 7.3.1a. Of the 50 valid sites, 32 had statistically significant trends, including all of the sites in the eastern United States. Sites in the Intermountain West and parts of California were associated with insignificant

and flat trends. Small positive but insignificant trends occurred at Bridger WA, Wyoming (BRID1), Jarbidge, Nevada (JARB1), Crater Lake NP, Oregon (CRLA1), Lassen Volcanic NP, California (LAVO1), and Bliss SP, California (BLIS1), all sites likely associated with impacts from biomass burning. The strongest statistically significant reductions in  $b_{\text{ext\_POM}}$  occurred at Mount Rainier NP, Washington (MORA1,  $-3.14\% \text{ yr}^{-1}$ ,  $p < 0.001$ ), and the least reduction occurred at Guadalupe Mountains, NP, Texas (GUMO1,  $-0.94\% \text{ yr}^{-1}$ ,  $p = 0.015$ ). Strong reductions at sites in the East occurred at Dolly Sods WA, West Virginia (DOSO1,  $-2.89\% \text{ yr}^{-1}$ ,  $p < 0.001$ ), Shenandoah NP, Virginia (SHEN1,  $-2.46\% \text{ yr}^{-1}$ ,  $p < 0.001$ ), and Moosehorn National Wildlife Refuge (NWR), Maine, (MOOS1,  $-2.88\% \text{ yr}^{-1}$ ,  $p < 0.001$ ).

With the addition of short-term sites, the area with sites having insignificant short-term trends expanded farther north (Figure 7.3.1b) into Montana, Idaho, and Washington, where biomass smoke has influenced trends in fine mass and organic carbon (McClure and Jaffe, 2018). All of the sites with insignificant trends occurred in the western United States and in Alaska, Hawaii, and the Virgin Islands. Of the 136 valid sites, 63 of them had statistically significant trends. The strongest reduction occurred at Agua Tibia, California (AGTI1,  $-4.27\% \text{ yr}^{-1}$ ,  $p < 0.001$ ), and the least reduction occurred at Big Bend NP, Texas (BIBE,  $-1.33\% \text{ yr}^{-1}$ ,  $p = 0.019$ ). Relatively strong reductions in annual mean  $b_{\text{ext\_POM}}$  occurred in the southeastern and northeastern United States, Arizona, New Mexico, and southern California.

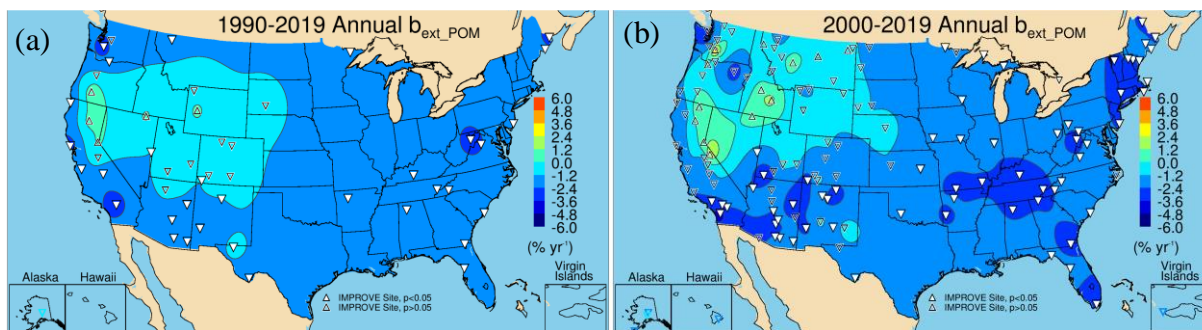


**Figure 7.3.1. Annual mean particulate organic matter  $b_{\text{ext}}$  ( $b_{\text{ext\_POM}}$ ) trends ( $\% \text{ yr}^{-1}$ ) for (a) long-term (1990–2019) and (b) short-term (2000–2019) periods. Filled triangles correspond to statistically significant trends ( $p \leq 0.05$ ).**

Regional seasonal mean  $b_{\text{ext\_POM}}$  trends are shown in Figure 7.3.2. Statistically significant trends occurred during all seasons in the Southeast, Northeast, and the Midsouth regions ( $\sim -3\% \text{ yr}^{-1}$ ). The strongest reductions in most of these regions occurred for winter and spring. Trends in the Central region were lower ( $\sim -1\% \text{ yr}^{-1}$  to  $-2\% \text{ yr}^{-1}$ ) than regions in the East and statistically significant in all seasons except summer. Seasonal mean trends in western regions were more variable than in regions in the East. All of the winter and spring trends were statistically significant, and  $b_{\text{ext\_POM}}$  declined more strongly in these seasons ( $-3\% \text{ yr}^{-1}$  to  $-4\% \text{ yr}^{-1}$ ). Summer and fall trends were insignificant and summer trends were flat in the Northwest and California regions. These seasons have been influenced by biomass burning emissions.

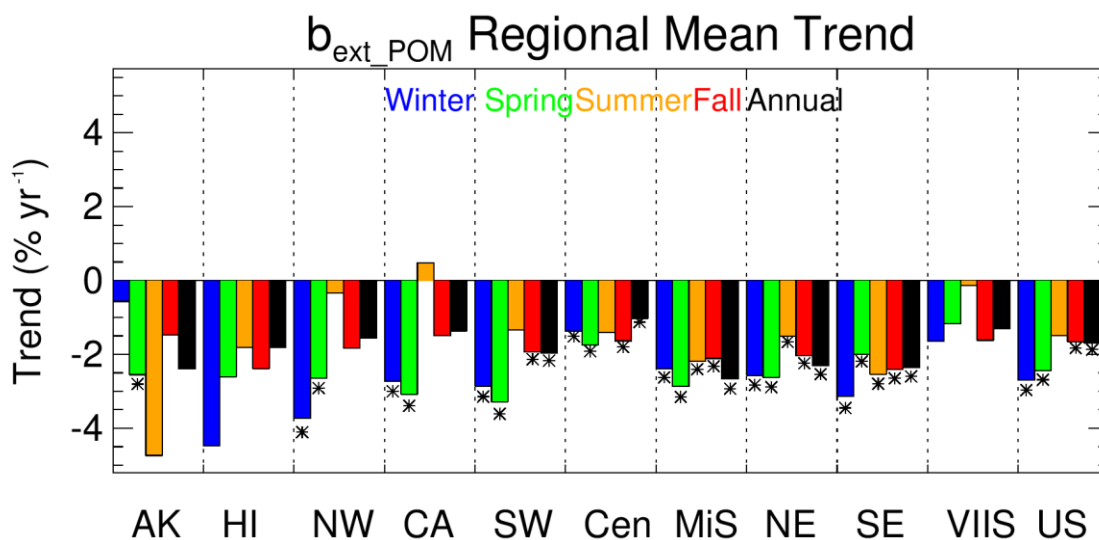
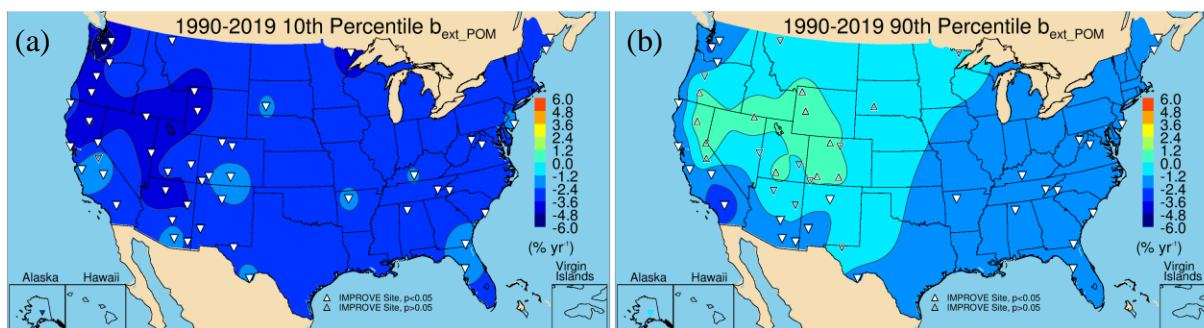


Figure 7.3.2. Short-term (2000–2019) regional, seasonal mean particulate organic matter  $b_{\text{ext\_POM}}$  trends ( $\% \text{ yr}^{-1}$ ) for major U.S. regions for winter, spring, summer, fall, and annual means. Regions are arranged from western to eastern United States (AK= Alaska, HI = Hawaii, NW = Northwest, CA= California, SW = Southwest, Cen = Central, MiS = Midsouth, NE = Northeast, SE = Southeast, VIIS = Virgin Islands, and US = all sites). Statistically significant trends ( $p \leq 0.05$ ) are denoted with “\*”.

Long-term trends in the 10<sup>th</sup> percentile and 90<sup>th</sup> percentile  $b_{\text{ext\_POM}}$  (Figure 7.3.3a and 7.3.3b, respectively) had different spatial patterns. At sites in the West, 10<sup>th</sup> percentile  $b_{\text{ext\_POM}}$  trends were much stronger than for the 90<sup>th</sup> percentile  $b_{\text{ext\_POM}}$  trends. Of the 50 long-term valid sites, 49 had statistically significant trends in 10<sup>th</sup> percentile  $b_{\text{ext\_POM}}$ . Strong reductions occurred at sites in northern California, Oregon, and Washington ( $-5\% \text{ yr}^{-1}$  to  $-6\% \text{ yr}^{-1}$ ), with the strongest at Mount Rainier NP, Washington (MORA1,  $-6.48\% \text{ yr}^{-1}$ ,  $p < 0.001$ ). However, some sites across the United States experienced reductions around  $-2\% \text{ yr}^{-1}$  or greater. The lowest reduction occurred at Great Sand Dunes NP, Colorado (GRSA1,  $-1.31\% \text{ yr}^{-1}$ ,  $p < 0.001$ ).

In contrast, long-term 90<sup>th</sup> percentile trends at sites across the western United States were mostly insignificant, with over half (27) of the sites meeting statistical significance. The strongest trend occurred at San Geronio WA, California (SAGO1,  $-3.50\% \text{ yr}^{-1}$ ,  $p < 0.001$ ), compared to the weakest at Bandalier NM, New Mexico (BAND1,  $-1.03\% \text{ yr}^{-1}$ ,  $p = 0.015$ ). These results suggest different influences on trends for low and high  $b_{\text{ext\_POM}}$ . The trends in the highest  $b_{\text{ext\_POM}}$  in the western United States were likely influenced by biomass burning impacts.



**Figure 7.3.3. IMPROVE long-term (1990–2019) trends (% yr<sup>-1</sup>) in (a) 10<sup>th</sup> percentile particulate organic matter  $b_{ext}$  ( $b_{ext\_POM}$ ) and (b) 90<sup>th</sup> percentile  $b_{ext\_POM}$ . Filled triangles correspond to statistically significant trends ( $p \leq 0.05$ ).**

Spatial patterns in short-term trends in the 10<sup>th</sup> and 90<sup>th</sup> percentile  $b_{ext\_POM}$  were similar to long-term trends (Figure 7.3.4a and 7.3.4b, respectively). Many of the 10<sup>th</sup> percentile trends were statistically significant (93 out of 138 valid sites) and nearly all of these sites were in the eastern United States. However, some of the strongest reductions in the 10<sup>th</sup> percentile  $b_{ext\_POM}$  occurred at sites in the West, such as Colorado, Wyoming, Nevada, Washington, and southern California. The greatest reductions occurred at North Absaroka, Wyoming (NOAB1,  $-8.37\% \text{ yr}^{-1}$ ,  $p = 0.003$ ), compared to Ike’s Backbone, Arizona (IKBA1,  $-1.70\% \text{ yr}^{-1}$ ,  $p = 0.002$ ).

Many of the short-term trends in the 90<sup>th</sup> percentile  $b_{ext\_POM}$  at sites in the West were insignificant, except for sites in southern California and Arizona (Figure 7.3.4b). Influences on the highest  $b_{ext\_POM}$  trends do not appear to be affecting the lowest  $b_{ext\_POM}$  over time. The strongest reductions in the 90<sup>th</sup> percentile trends occurred at Sierra Ancha, Arizona (SIAN1,  $-4.16\% \text{ yr}^{-1}$ ,  $p = 0.009$ ), compared to  $-1.31\% \text{ yr}^{-1}$  ( $p = 0.016$ ) at Moosehorn NWR, Maine (MOOS1). Although all insignificant, 22 trends were positive.

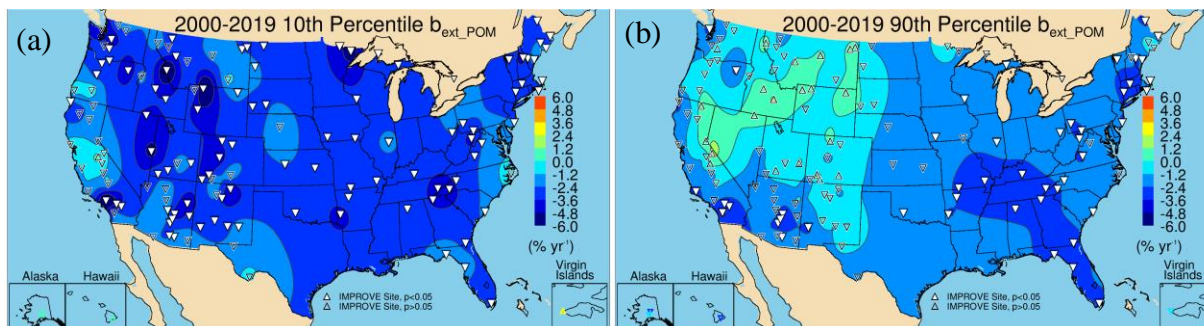


**Figure 7.3.4. IMPROVE short-term (2000–2019) trends (% yr<sup>-1</sup>) in (a) 10<sup>th</sup> percentile particulate organic matter  $b_{ext}$  ( $b_{ext\_POM}$ ) and (b) 90<sup>th</sup> percentile  $b_{ext\_POM}$ . Filled triangles correspond to statistically significant trends ( $p \leq 0.05$ ).**

Comparisons of regional mean percentile trends are shown in Figure 7.3.5. The 90<sup>th</sup> percentile trends were the weakest and statistically insignificant for regions in the West, such as the Northwest, California, and the Southwest regions. The 10<sup>th</sup> percentile trends in the California region were also insignificant. For the Southeast region, the range in trends for different percentiles was low. Almost all regions had stronger reductions in the 10<sup>th</sup> percentile  $b_{ext\_POM}$  relative to other percentile trends.

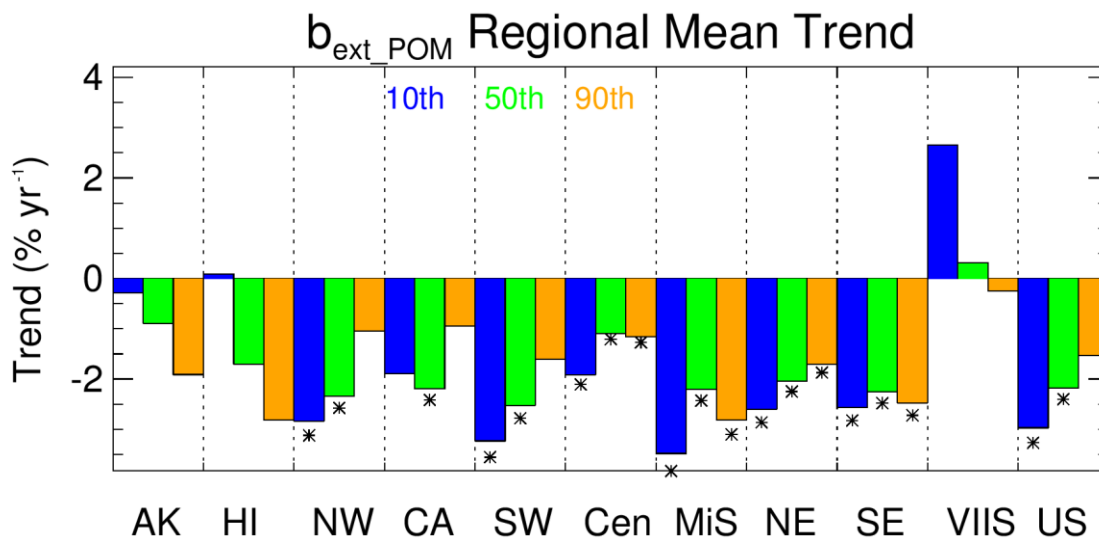
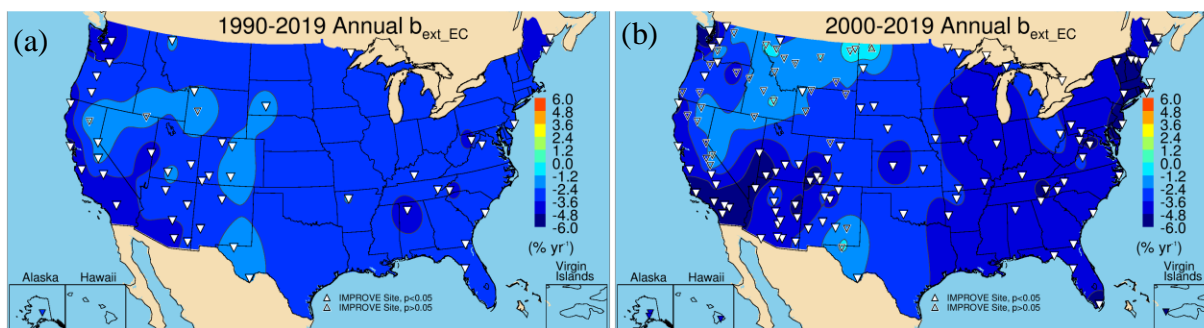


Figure 7.3.5. Short-term (2000–2019) regional mean trends ( $\% \text{ yr}^{-1}$ ) in 10<sup>th</sup>, 50<sup>th</sup>, and 90<sup>th</sup> percentile particulate organic matter  $b_{ext}$  ( $b_{ext\_POM}$ ). Regions are arranged from western to eastern United States (AK = Alaska, HI = Hawaii, NW = Northwest, CA = California, SW = Southwest, Cen = Central, MiS = Midsouth, NE = Northeast, SE = Southeast, VIIS = Virgin Islands, and US = all sites). Statistically significant trends ( $p \leq 0.05$ ) are denoted with “\*”.

#### 7.4 ELEMENTAL CARBON LIGHT EXTINCTION COEFFICIENT TRENDS

Long-term trends in annual mean  $b_{ext\_EC}$  are shown in Figure 7.4.1a. Of the 50 valid trends, 47 were statistically significant, and all were negative. The strongest reduction occurred at Point Reyes NP, California (PORE1,  $-5.73\% \text{ yr}^{-1}$ ,  $p < 0.001$ ), compared to the weakest at Guadalupe Mountains NP, Texas (GUMO1,  $-1.45\% \text{ yr}^{-1}$ ,  $p < 0.001$ ). The weakest trends occurred at sites in the West, and sites with insignificant trends occurred in areas influenced by biomass smoke (Bridger WA, Wyoming, BRID1; Jarbidge WA, Nevada, JARB1; and Lassen Volcanic NP, LAVO1).

Of the 136 valid short-term sites, 103 had statistically significant negative trends (Figure 7.4.1b). Sites with the strongest reductions ( $-5\% \text{ yr}^{-1}$  to  $-6\% \text{ yr}^{-1}$ ) were in southern California, the northwestern United States, and regions of the northeastern United States. The Moosehorn NWR, Maine (MOOS1), site had the strongest reduction in  $b_{ext\_EC}$  ( $-7.77\% \text{ yr}^{-1}$ ,  $p < 0.001$ ) compared to the weakest at White Mountain, New Mexico (WHIT1,  $-2.14\% \text{ yr}^{-1}$ ,  $p = 0.03$ ). Most of the statistically insignificant trends occurred in the West at sites influenced by biomass smoke and in northern Montana and North Dakota, where oil and gas development has been demonstrated to impact EC concentrations (Gebhart et al., 2018).



**Figure 7.4.1. Annual mean elemental carbon  $b_{ext}$  ( $b_{ext\_EC}$ ) trends for (a) long-term (1990–2019) and (b) short-term (2000–2019) periods. Filled triangles correspond to statistically significant trends ( $p \leq 0.05$ ).**

A summary of short-term regional seasonal mean trends is shown in Figure 7.4.2. Negative trends occurred for all regions and seasons, with large ranges in trends for some regions. Some of the strongest reductions occurred during all seasons in the Virgin Islands region. In eastern regions, the largest negative trends occurred during summer ( $\sim -5\% \text{ yr}^{-1}$ ). Trends in the Southeast region were somewhat larger than in other eastern regions and were large in both winter and summer. The lowest negative trends occurred in the Central region, especially in winter ( $-1.89\% \text{ yr}^{-1}$ ). In the West, the strongest reductions in  $b_{ext\_EC}$  ( $\sim -6\% \text{ yr}^{-1}$ ) occurred mainly in winter and spring (e.g., California) and were larger than regional trends in the East. Trends for all western regions were lowest in the summer and in the Northwest were insignificant, likely reflecting the role of biomass smoke on  $b_{ext\_EC}$ . The difference in seasonal and regional trends implies different sources and temporal behavior on  $b_{ext\_EC}$  depending on location.

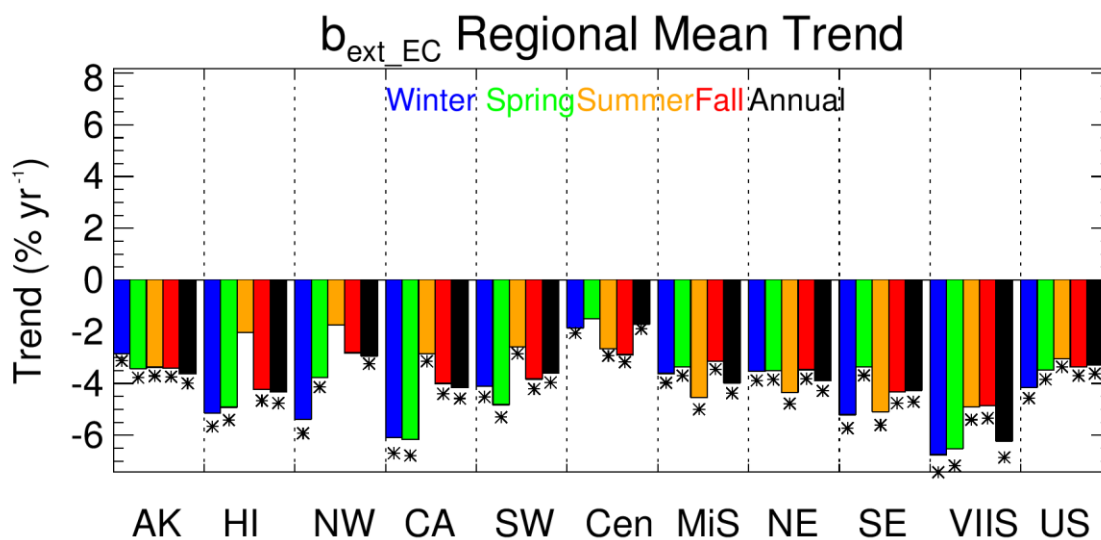


**Figure 7.4.2. Short-term (2000–2019) regional seasonal mean elemental carbon  $b_{ext}$  ( $b_{ext\_EC}$ ) trends ( $\% \text{ yr}^{-1}$ ) for major U.S. regions for winter, spring, summer, fall, and annual means. Regions are arranged from western to eastern United States (AK = Alaska, HI = Hawaii, NW = Northwest, CA = California, SW = Southwest, Cen = Central, MiS = Midsouth, NE = Northeast, SE = Southeast, VIIS = Virgin Islands, and US = all sites). Statistically significant trends ( $p \leq 0.05$ ) are denoted with “\*”.**

Long-term trends in 10<sup>th</sup> and 90<sup>th</sup> percentile  $b_{\text{ext\_EC}}$  are shown in Figure 7.4.3a and 7.4.3b, respectively. The strongest reductions in the 10<sup>th</sup> percentile  $b_{\text{ext\_EC}}$  occurred at sites in the western United States. Of the 51 valid sites, all had statistically significant trends. The largest negative trend occurred at Three Sisters WA, Oregon (THSI1,  $-9.29\% \text{ yr}^{-1}$ ,  $p < 0.001$ ), compared to the weakest trend at Glacier NP, Montana (GLAC1,  $-2.16\% \text{ yr}^{-1}$ ,  $p = 0.002$ ).

The 90<sup>th</sup> percentile  $b_{\text{ext\_EC}}$  declined at all of the valid long-term sites, with 46 of the 51 sites having statistically significant trends (Figure 7.4.3b). The strongest reductions were around  $-4\% \text{ yr}^{-1}$  to  $-5\% \text{ yr}^{-1}$  at sites in the northwestern United States, northeastern United States, and southern California. The strongest trend occurred at Point Reyes NP, California (PORE1,  $-5.46\% \text{ yr}^{-1}$ ,  $p < 0.001$ ), and the weakest at Great Sand Dunes NP, Colorado (GRSA1,  $-1.00\% \text{ yr}^{-1}$ ,  $p = 0.02$ ). Sites in Intermountain West and parts of California and Texas had weak and insignificant trends.

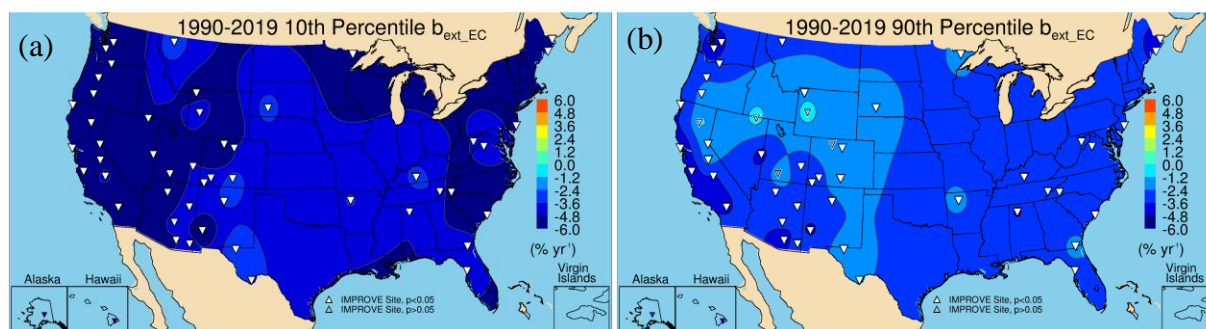


**Figure 7.4.3. IMPROVE long-term (1990–2019) trends ( $\% \text{ yr}^{-1}$ ) in (a) 10<sup>th</sup> percentile elemental carbon  $b_{\text{ext}}$  ( $b_{\text{ext\_EC}}$ ) and (b) 90<sup>th</sup> percentile  $b_{\text{ext\_EC}}$ . Filled triangles correspond to statistically significant trends ( $p \leq 0.05$ ).**

Negative short-term trends in 10<sup>th</sup> percentile  $b_{\text{ext\_EC}}$  occurred at all sites except Lostwood, North Dakota (LOST1), which was insignificant (Figure 7.4.4a). Recall that EC concentrations at many sites, especially in the West, may be below the lower quantifiable limit (LQL), and therefore 10<sup>th</sup> percentile trends in  $b_{\text{ext\_EC}}$  may be more uncertain. The strongest reduction occurred at Starkey, Oregon (STAR1,  $-13.79\% \text{ yr}^{-1}$ ,  $p < 0.001$ ), compared to  $-2.25\% \text{ yr}^{-1}$  ( $p = 0.04$ ) at Big Bend NP, Texas (BIBE1). Short-term trends in the 90<sup>th</sup> percentile  $b_{\text{ext\_EC}}$  are shown in Figure 7.4.4b. Insignificant trends occurred at sites across the Intermountain West and northwestern United States. Some of these sites may be influenced by biomass smoke, and some, such as Theodore Roosevelt NP, North Dakota (THRO1), may be influenced by oil and gas development (Gebhart et al., 2018). Out of the 138 valid sites, 129 had statistically significant trends. Strong reductions in the 90<sup>th</sup> percentile  $b_{\text{ext\_EC}}$  occurred at sites in southern California and the northeastern and northwestern United States. Short-term 90<sup>th</sup> percentile trends ranged from  $-7.56\% \text{ yr}^{-1}$  ( $p < 0.001$ ) at San Geronio WA, California (SAGO1), to  $-1.92\% \text{ yr}^{-1}$  ( $p = 0.04$ ) at Theodore Roosevelt NP, North Dakota (THRO1).

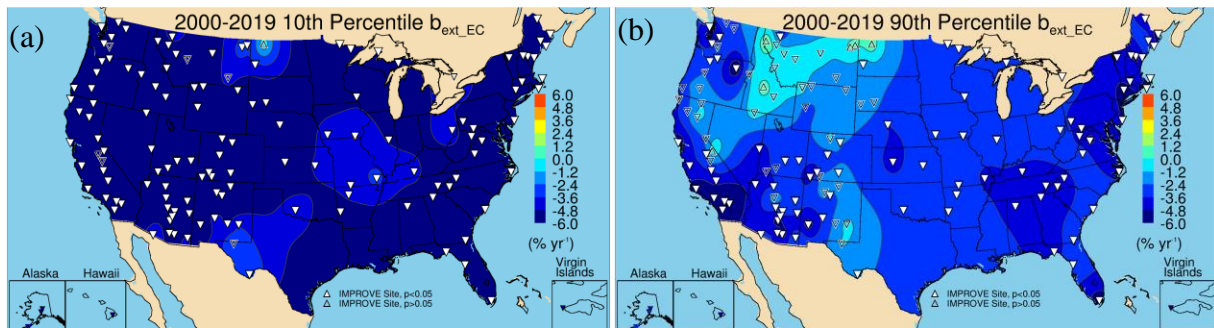


Figure 7.4.4. IMPROVE short-term (2000–2019) trends ( $\% \text{ yr}^{-1}$ ) in (a) 10<sup>th</sup> percentile elemental carbon  $b_{\text{ext\_EC}}$  ( $b_{\text{ext\_EC}}$ ) and (b) 90<sup>th</sup> percentile  $b_{\text{ext\_EC}}$ . Filled triangles correspond to statistically significant trends ( $p \leq 0.05$ ).

Regional mean trends in percentile  $b_{\text{ext\_EC}}$  are shown in Figure 7.4.5. For nearly all regions, the 10<sup>th</sup> percentile trends were the greatest, although these were likely affected by low  $b_{\text{ext\_EC}}$  (e.g., Alaska, Hawaii, and Virgin Islands). For most regions, the 90<sup>th</sup> percentile  $b_{\text{ext\_EC}}$  decreased at a lower rate than the median  $b_{\text{ext\_EC}}$ . Both the Northwest and Alaska regions had insignificant trends in 90<sup>th</sup> percentile  $b_{\text{ext\_EC}}$ , perhaps related to increased smoke impacts.

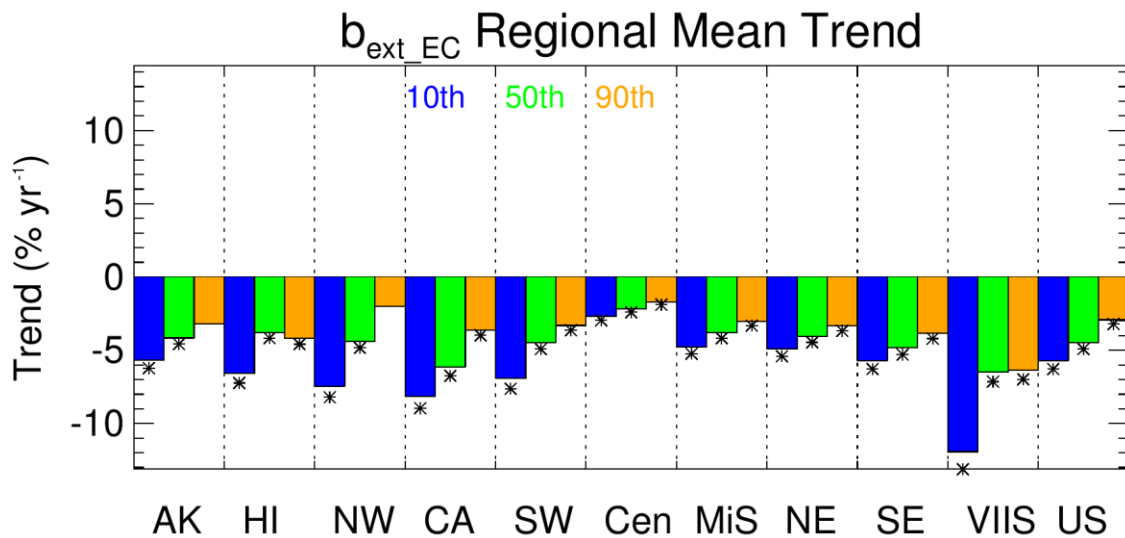


Figure 7.4.5. Short-term (2000–2019) regional mean trends ( $\% \text{ yr}^{-1}$ ) in 10<sup>th</sup>, 50<sup>th</sup>, and 90<sup>th</sup> percentile elemental carbon  $b_{\text{ext}}$  ( $b_{\text{ext\_EC}}$ ). Regions are arranged from western to eastern United States (AK = Alaska, HI = Hawaii, NW = Northwest, CA = California, SW = Southwest, Cen = Central, MiS = Midsouth, NE = Northeast, SE = Southeast, VIIS = Virgin Islands, and US = all sites). Statistically significant trends ( $p \leq 0.05$ ) are denoted with “\*”.

## 7.5 FINE DUST LIGHT EXTINCTION COEFFICIENT TRENDS

Long-term and short-term annual mean  $b_{\text{ext\_FD}}$  trends are shown in Figures 7.5.1a and 7.5.1b, respectively. Many of the long-term trends were statistically insignificant, nearly all of these were located at sites in the western United States, and many of them were positive. In the West, statistically significant reductions in  $b_{\text{ext\_FD}}$  occurred at sites in California, Oregon, Washington State, Wyoming, and Colorado. Across the eastern United States, sites were

associated with reduced  $b_{\text{ext\_FD}}$ , although with some insignificant trends. The strongest reductions occurred at Yellowstone NP, Wyoming (YELL2,  $-3.94\% \text{ yr}^{-1}$ ,  $p < 0.001$ ), compared to an increase in annual mean  $b_{\text{ext\_FD}}$  at Guadalupe Mountains NP, Texas (GUMO1,  $1.22\% \text{ yr}^{-1}$ ,  $p = 0.05$ ).

Annual mean trends in  $b_{\text{ext\_FD}}$  for 2000 to 2019 were significantly negative across the eastern United States, especially at sites in the northeastern United States and across the Intermountain West and northwestern United States (Figure 7.5.1b). Out of 137 sites, 62 had statistically significant trends. These ranged from  $-7.12\% \text{ yr}^{-1}$  ( $p < 0.001$ ) at Mohawk Mountain, Connecticut (MOMO1), to  $-2.40\% \text{ yr}^{-1}$  ( $p = 0.03$ ) at Northern Cheyenne, Montana (NOCH1). Many sites near the Central Valley of California, Oklahoma, Texas, Oregon, and North Dakota had positive but insignificant trends. Many of the sites in the southwestern United States corresponded to statistically insignificant negative trends.

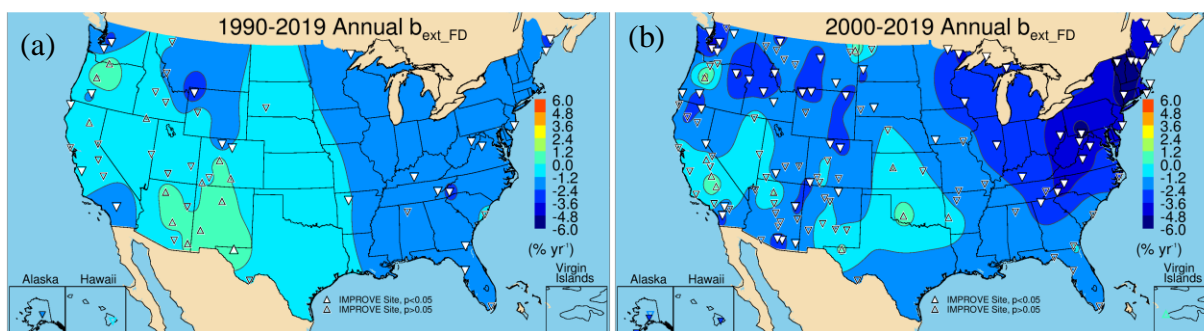


**Figure 7.5.1 Annual mean fine dust  $b_{\text{ext}}$  ( $b_{\text{ext\_FD}}$ ) trends ( $\% \text{ yr}^{-1}$ ) for (a) long-term (1990–2019) and (b) short-term (2000–2019) periods. Filled triangles correspond to statistically significant trends ( $p \leq 0.05$ ).**

Compared to other species, regional seasonal mean trends in  $b_{\text{ext\_FD}}$  showed greater variability. Trends were mostly insignificant and generally not strongly negative as was the case for other species. The Northeast region was the only region with statistically significant trends during all seasons ( $-3\% \text{ yr}^{-1}$  to  $-5\% \text{ yr}^{-1}$ ). The Southeast region had statistically significant reductions in  $b_{\text{ext\_FD}}$  during all seasons except summer. Similarly, the Midsouth region had insignificant but positive trends during summer; this is the season with impacts from North African dust transport. In the Central region, only winter and spring corresponded to statistically significant negative trends ( $\sim -2\% \text{ yr}^{-1}$ ). Across the West, regions were associated with insignificant though negative trends. The California region had insignificant but positive trends during fall. The levels of progress that have been observed in reducing extinction from other species have not been experienced by  $b_{\text{ext\_FD}}$ .

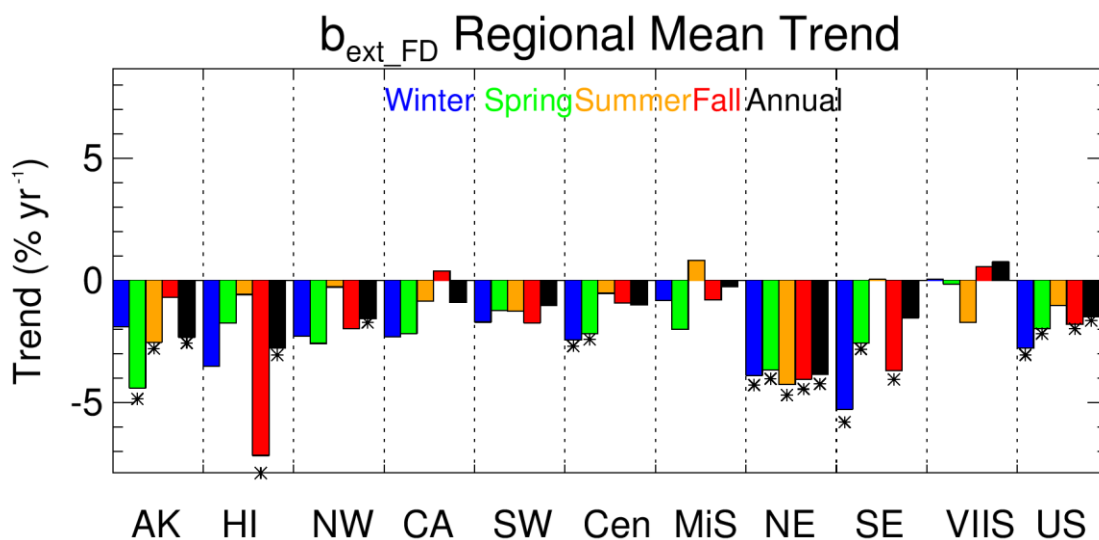


Figure 7.5.2. Short-term (2000–2019) regional seasonal mean fine dust  $b_{ext}$  ( $b_{ext\_FD}$ ) trends ( $\% \text{ yr}^{-1}$ ) for major U.S. regions for winter, spring, summer, fall, and annual means. Regions are arranged from western to eastern United States (AK = Alaska, HI = Hawaii, NW = Northwest, CA = California, SW = Southwest, Cen = Central, MiS = Midsouth, NE = Northeast, SE = Southeast, VIIS = Virgin Islands, and US = all sites). Statistically significant trends ( $p \leq 0.05$ ) are denoted with “\*”.

Long-term trends in the 10<sup>th</sup> percentile  $b_{ext\_FD}$  are shown in Figure 7.5.3a. For most of the United States, sites experienced reductions in the lowest  $b_{ext\_FD}$ . Of the 59 valid sites, 46 had statistically significant trends, ranging from  $-5.97\% \text{ yr}^{-1}$  ( $p < 0.001$ ) in Three Sisters WA, Oregon (THS11), to  $1.80\% \text{ yr}^{-1}$  ( $p = 0.010$ ) in Guadalupe Mountains NP, Texas (GUMO1). All of the insignificant trends occurred in the southwestern United States. In contrast, for the 90<sup>th</sup> percentile  $b_{ext\_FD}$ , of the 59 valid sites only 17 had statistically significant trends, and many of these were in the eastern United States (Figure 7.5.3b). Sites across the southwestern United States were associated with positive although insignificant trends. Trends ranged from  $-3.78\% \text{ yr}^{-1}$  ( $p < 0.001$ ) at Yellowstone NP, Wyoming (YELL2), to  $2.38\% \text{ yr}^{-1}$  ( $p = 0.012$ ) at Columbia River Gorge, Washington (COR11).

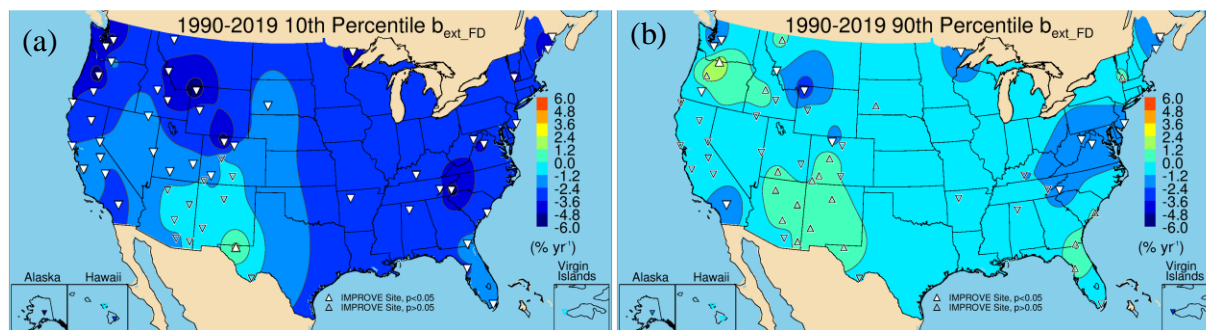
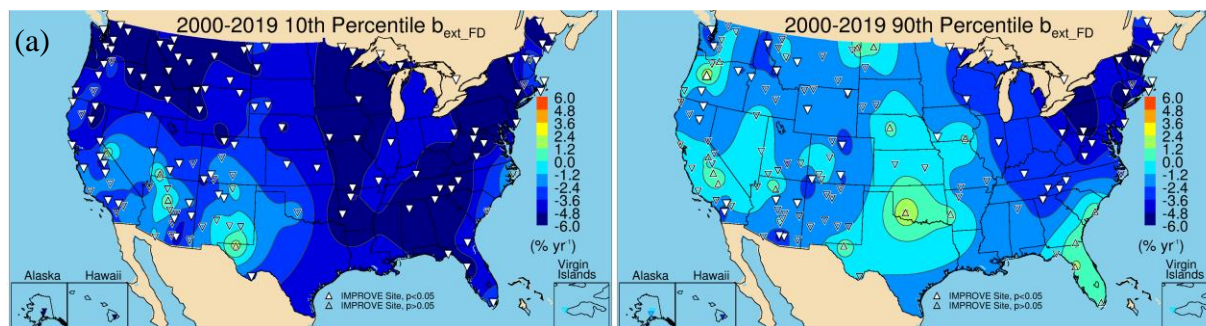


Figure 7.5.3. IMPROVE long-term (1990–2019) trends ( $\% \text{ yr}^{-1}$ ) in (a) 10<sup>th</sup> percentile fine dust  $b_{ext}$  ( $b_{ext\_FD}$ ) and (b) 90<sup>th</sup> percentile  $b_{ext\_FD}$ . Filled triangles correspond to statistically significant trends ( $p \leq 0.05$ ).

Short-term trends in 10<sup>th</sup> percentile  $b_{ext\_FD}$  were negative at sites across the United States, with stronger reductions at sites across the eastern United States, Intermountain West, and

northwestern United States, but with several sites having insignificant trends in the Southwest. Insignificant trends occurred at 34 sites (out of 137), and most of these were in the southwestern United States (Figure 7.5.4a). Trends ranged from  $-8.59\% \text{ yr}^{-1}$  ( $p < 0.001$ ) at Shining Rock WA, North Carolina (SHRO1), to  $-1.72\% \text{ yr}^{-1}$  ( $p = 0.019$ ) at Pinnacles NM, California (PINN1). Most of the 90<sup>th</sup> percentile  $b_{\text{ext\_FD}}$  trends in the West were insignificant (Figure 7.5.4b), with 83 insignificant trends. Positive though insignificant trends occurred at sites in the central United States, the Central Valley of California, Oregon, the northern Great Plains, and Florida. The 90<sup>th</sup> percentile trends ranged from  $-6.67\% \text{ yr}^{-1}$  ( $p < 0.001$ ) at Great Gulf WA, New Hampshire (GRGU1), to  $2.87\% \text{ yr}^{-1}$  ( $p = 0.03$ ) at Three Sisters WA, Oregon (THSI1). Comparison of trends from these two maps suggests that the influences that govern the changes in the 10<sup>th</sup> and 90<sup>th</sup> percentiles are different, although low 10<sup>th</sup> percentile  $b_{\text{ext\_FD}}$  could also play a role.



**Figure 7.5.4. IMPROVE short-term (2000–2019) trends ( $\% \text{ yr}^{-1}$ ) in (a) 10<sup>th</sup> percentile fine dust  $b_{\text{ext}}$  ( $b_{\text{ext\_FD}}$ ) and (b) 90<sup>th</sup> percentile  $b_{\text{ext\_FD}}$ . Filled triangles correspond to statistically significant trends ( $p \leq 0.05$ ).**

Regional mean percentile trends are shown in Figure 7.5.5. For most regions, the 10<sup>th</sup> percentile trends were strongest, which may be in part due to low 10<sup>th</sup> percentile  $b_{\text{ext\_FD}}$ . For nearly all regions, the 90<sup>th</sup> percentile trends were insignificant (except the Northeast and Hawaii regions). These insignificant trends may imply that the influences on the highest  $b_{\text{ext\_FD}}$  have not decreased enough to result in statistically significant negative trends. For other regions in the West, such as California, Southwest, and Central, the median trends were also insignificant.

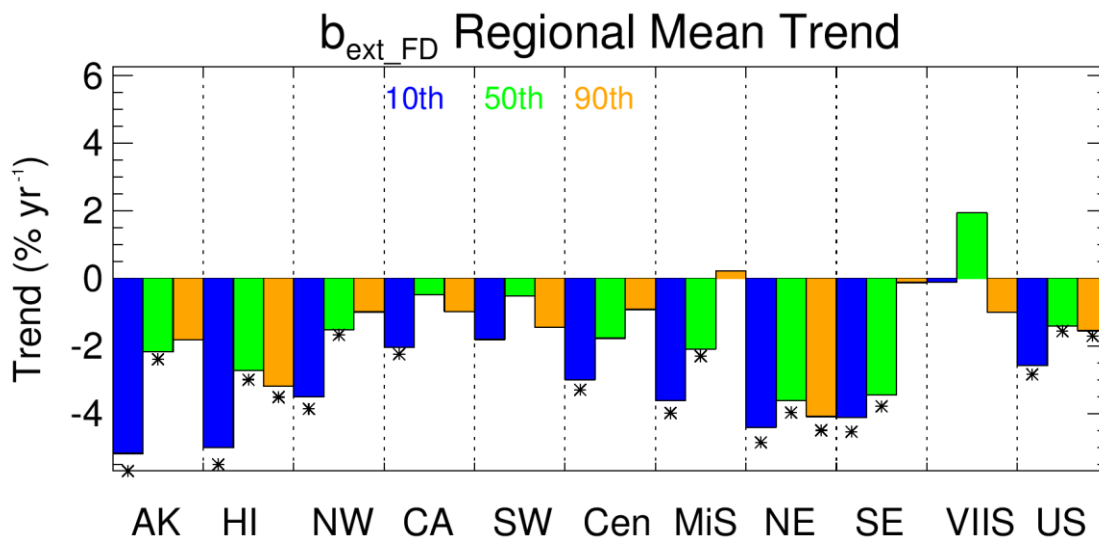


Figure 7.5.5. Short-term (2000–2019) regional mean trends (%yr<sup>-1</sup>) in 10<sup>th</sup>, 50<sup>th</sup>, and 90<sup>th</sup> percentile fine dust  $b_{ext\_FD}$ . Regions are arranged from western to eastern United States (AK = Alaska, HI = Hawaii, NW = Northwest, CA = California, SW = Southwest, Cen = Central, MiS = Midsouth, NE = Northeast, SE = Southeast, VIIS = Virgin Islands, and US = all sites). Statistically significant trends ( $p \leq 0.05$ ) are denoted with “\*”.

## 7.6 COARSE MASS LIGHT EXTINCTION COEFFICIENT TRENDS

Annual mean long-term trends in  $b_{ext\_CM}$  are shown in Figure 7.6.1a. The strongest reductions in  $b_{ext\_CM}$  occurred at sites in Wyoming, Colorado, and Oregon. Of the 49 valid sites, 30 had statistically significant trends. Insignificant trends mostly occurred in the western United States, at sites in California, Arizona, and Texas. One positive trend occurred at Columbia River Gorge, Washington (CORI1, 1.83% yr<sup>-1</sup>,  $p = 0.04$ ). The strongest reduction in  $b_{ext\_CM}$  occurred at Crater Lake NP, Oregon (CRLA1, -5.39% yr<sup>-1</sup>,  $p < 0.001$ ).

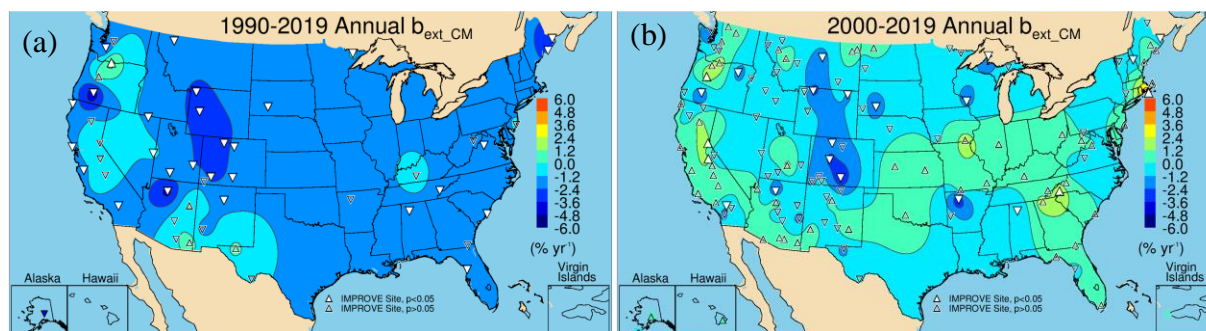
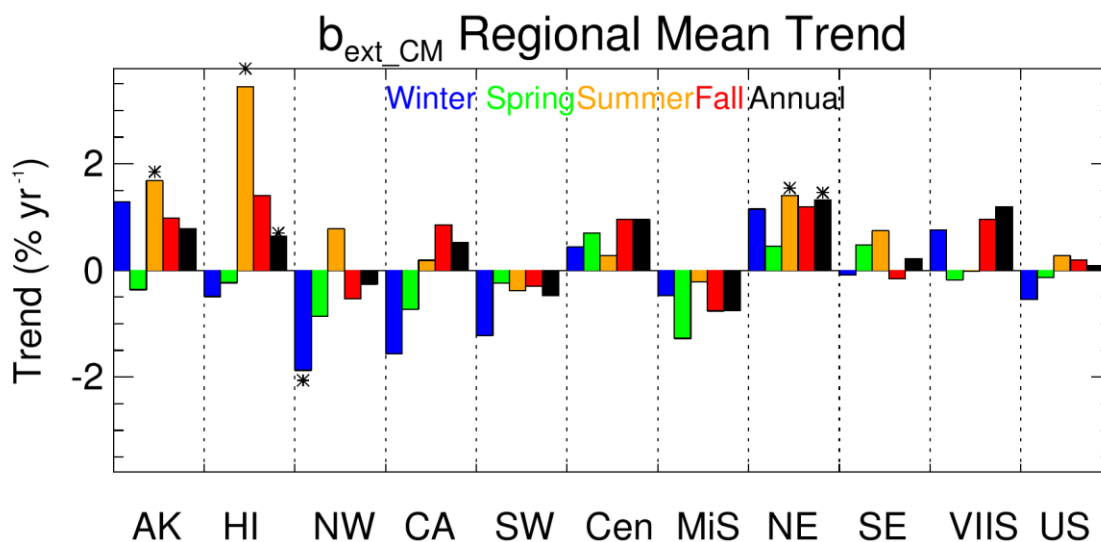


Figure 7.6.1. Annual mean coarse mass  $b_{ext\_CM}$  trends (% yr<sup>-1</sup>) for (a) long-term (1990–2019) and (b) short-term (2000–2019) periods. Filled triangles correspond to statistically significant trends ( $p \leq 0.05$ ).

Short-term annual mean  $b_{ext\_CM}$  trends are shown in Figure 7.6.1b. Only 24 of 131 valid sites had statistically significant trends, suggesting that at most sites, trends were variable. Significant reductions in  $b_{ext\_CM}$  occurred at sites in Colorado, Wyoming, Montana, and Arkansas, where the strongest reductions occurred at Upper Buffalo WA, Arkansas

(UPBU1,  $-3.92\% \text{ yr}^{-1}$ ,  $p = 0.037$ ). Positive trends (mostly insignificant) occurred at 61 sites, with seven being statistically significant (Martha’s Vineyard, Massachusetts, MAVI1; Shining Rock WA, North Carolina, SHRO1; Three Sisters WA, Oregon, THSI1; Yosemite NP, California, YOSE1; Bliss SP, California, BLIS1; Trapper Creek, Alaska, TRCR1; and Hawaii Volcanoes NP, Hawaii, HAVO1). The spatial pattern in short-term  $b_{\text{ext\_CM}}$  trends was different from  $b_{\text{ext\_FD}}$  trends (Figure 7.5.1b), suggesting that different composition or size distribution of coarse-mode aerosols influenced  $b_{\text{ext\_CM}}$  trends.

Regional seasonal mean trends are shown in Figure 7.6.2. As suggested in Figure 7.6.1b, nearly all of the regions were associated with insignificant and weak trends, especially relative to other species already discussed. The Northeast region had significant positive trends in summer, as did the Alaska and Hawaii regions. All of the seasonal mean trends in the Central region were positive but insignificant. The Midsouth and Southwest regions had weak but negative insignificant trends, while the California region had weak, positive insignificant trends in summer and fall but negative insignificant trends in winter and spring. The Northwest region had statistically significant trends in winter but weak and insignificant trends during other seasons.



**Figure 7.6.2.** Short-term (2000–2019) regional seasonal mean coarse mass  $b_{\text{ext}}$  ( $b_{\text{ext\_CM}}$ ) trends ( $\% \text{ yr}^{-1}$ ) for major U.S. regions for winter, spring, summer, fall, and annual means. Regions are arranged from western to eastern United States (AK = Alaska, HI = Hawaii, NW = Northwest, CA = California, SW = Southwest, Cen = Central, MiS = Midsouth, NE = Northeast, SE = Southeast, VIIS = Virgin Islands, and US = all sites). Statistically significant trends ( $p \leq 0.05$ ) are denoted with “\*”.

The long-term 10<sup>th</sup> percentile trends in  $b_{\text{ext\_CM}}$  were negative at most sites, with the strongest reductions at sites in the Intermountain West and southwestern United States (Figure 7.6.3a). Of the 50 valid sites, 31 had statistically significant trends, ranging from  $-8.94\% \text{ yr}^{-1}$  ( $p < 0.001$ ) at Mount Zirkel WA, Colorado (MOZI1), to  $-1.64\% \text{ yr}^{-1}$  ( $p = 0.016$ ) at Tonto NM, Arizona (TONT1). The trends in 90<sup>th</sup> percentile  $b_{\text{ext\_CM}}$  did not decrease to the same degree as the 10<sup>th</sup> percentile trends (Figure 7.6.3b). Of the 50 valid sites, 30 had statistically significant trends, ranging from  $-5.32\% \text{ yr}^{-1}$  ( $p < 0.001$ ) at Crater Lake NP, Oregon (CRLA1), to  $2.82\% \text{ yr}^{-1}$  ( $p = 0.002$ ) at Columbia River Gorge, Washington (COR11). Recall that the 90<sup>th</sup> percentile trend

in  $b_{\text{ext\_FD}}$  at CRLA1 was also positive, suggesting CM is likely associated with mineral dust at this site. The 90<sup>th</sup> percentile CM trends decreased more than the 90<sup>th</sup> percentile  $b_{\text{ext\_FD}}$  trends, especially for sites in the southwestern United States. Similarities in trends of  $b_{\text{ext\_FD}}$  and  $b_{\text{ext\_CM}}$  occurred for sites in Arizona and Texas. Sites in California had positive (insignificant)  $b_{\text{ext\_CM}}$  trends but negative  $b_{\text{ext\_FD}}$  90<sup>th</sup> percentile trends.

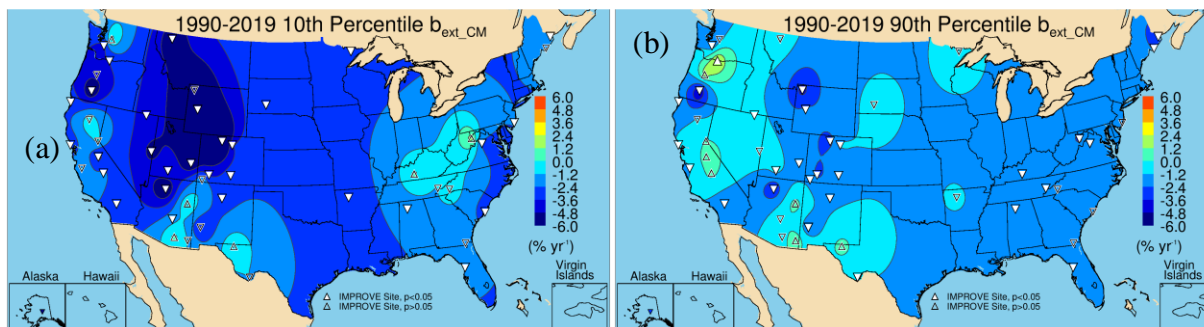


**Figure 7.6.3. IMPROVE long-term (1990–2019) trends ( $\% \text{ yr}^{-1}$ ) in (a) 10<sup>th</sup> percentile coarse mass  $b_{\text{ext}}$  ( $b_{\text{ext\_CM}}$ ) and (b) 90<sup>th</sup> percentile  $b_{\text{ext\_CM}}$ . Filled triangles correspond to statistically significant trends ( $p \leq 0.05$ ).**

Short-term trends in the 10<sup>th</sup> and 90<sup>th</sup> percentile  $b_{\text{ext\_CM}}$  (Figure 7.6.4a and 7.6.4b, respectively) showed more spatial variability than the long-term trends, with many more sites having insignificant and positive trends. The 10<sup>th</sup> percentile trends had only 22 statistically significant trends out of 137 valid sites. The strongest statistically insignificant negative trends occurred at sites in Colorado and Montana and parts of southern California and Oregon. Statistically significant positive trends occurred at several sites, with the strongest ( $>3\% \text{ yr}^{-1}$ ) at Shining Rock WA, North Carolina (SHRO1); Dolly Sods WA, West Virginia (DOSO1); Cohutta, Georgia (COHU1); Lassen Volcanic NP, California (LAVO1); and Pasayten, Washington (PASA1). Trends ranged from  $-9.50\% \text{ yr}^{-1}$  ( $p = 0.025$ ) at Gates of the Mountains, Montana (GAMO1), to  $7.66\% \text{ yr}^{-1}$  ( $p = 0.006$ ) at Shining Rock WA, North Carolina (SHRO1). Some of these trends may be affected by low  $b_{\text{ext\_CM}}$ .

Similar spatial patterns were seen for the short-term 90<sup>th</sup> percentile trends, with sites in the central United States, California, the Northwest, and the Southeast having positive but insignificant trends (Figure 7.6.4b). Sites with strongly decreased  $b_{\text{ext\_CM}}$  included those in Colorado. Of the 137 sites, 21 were statistically significant and ranged from  $-4.77\% \text{ yr}^{-1}$  ( $p = 0.005$ ) at Upper Buffalo WA, Arkansas (UPBU1), to  $5.31\% \text{ yr}^{-1}$  ( $p = 0.004$ ) at Martha's Vineyard, Massachusetts (MAVI1). Several of the sites with significant positive 10<sup>th</sup> percentile trends also had positive 90<sup>th</sup> percentile trends, such as Shining Rock WA, North Carolina (SHRO1); Cohutta, Georgia (COHU1); and Bliss SP, California (BLIS1). The short-term 10<sup>th</sup> and 90<sup>th</sup> percentiles trend maps did not reflect the corresponding  $b_{\text{ext\_FD}}$  trend maps, with the  $b_{\text{ext\_CM}}$  trends having much larger variability, more insignificant trends, and fewer sites with decreased trends.

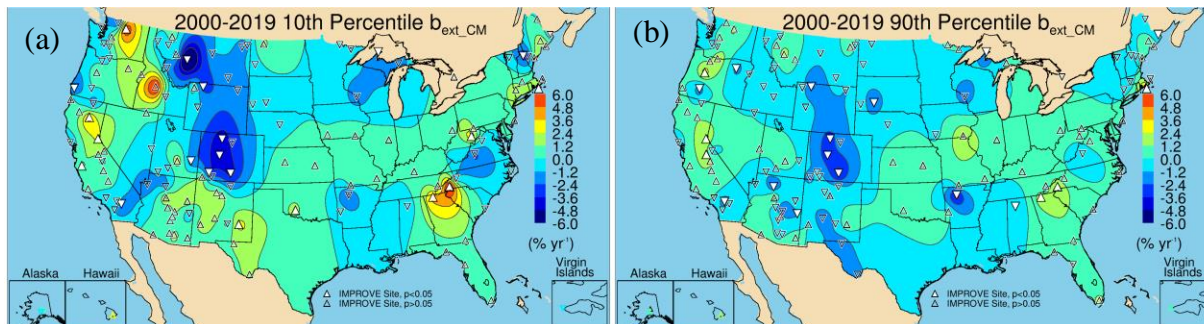


Figure 7.6.4. IMPROVE short-term (2000–2019) trends (%yr<sup>-1</sup>) in (a) 10<sup>th</sup> percentile coarse mass  $b_{ext\_CM}$  and (b) 90<sup>th</sup> percentile  $b_{ext\_CM}$ . Filled triangles correspond to statistically significant trends ( $p \leq 0.05$ ).

Comparisons of short-term regional mean percentile  $b_{ext\_CM}$  trends are shown in Figure 7.6.5. Unlike the results for  $b_{ext\_FD}$  trends (Figure 7.5.5), most of the regional mean trends are statistically insignificant, except for the positive 50<sup>th</sup> percentile trend in the Northeast region. The Central region had positive trends for all percentiles, although insignificant, while the Midsouth region had negative trends. The California region had weak to positive trends. Both the Hawaii and Alaska regions had positive but insignificant trends. Trends in  $b_{ext\_CM}$  were notable and indicated that  $b_{ext\_CM}$  has not decreased across large regions of the United States, unlike trends in extinction from other species.

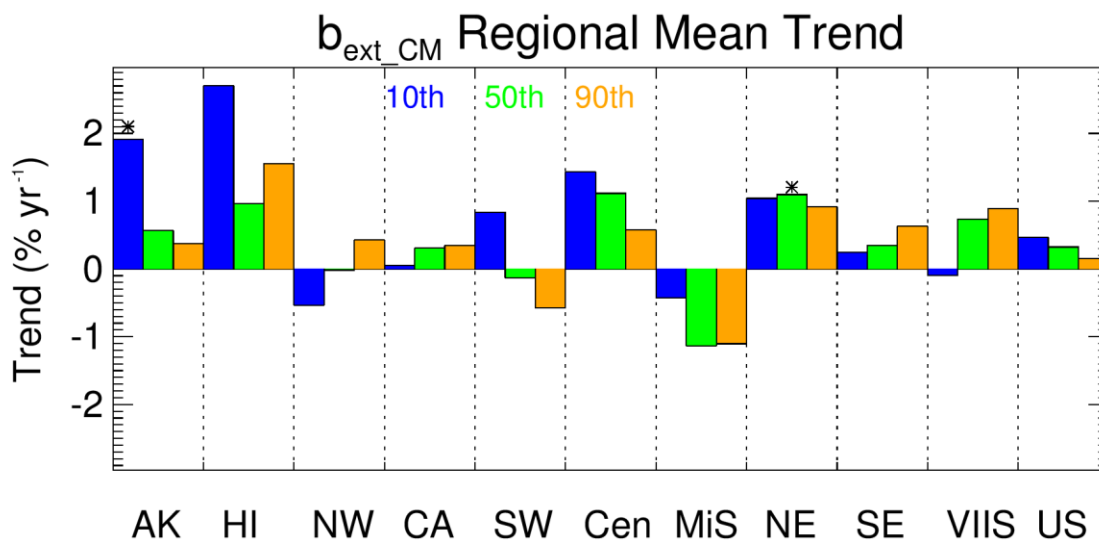


Figure 7.6.5. Short-term (2000–2019) regional mean trends (% yr<sup>-1</sup>) in 10<sup>th</sup>, 50<sup>th</sup>, and 90<sup>th</sup> percentile coarse mass  $b_{ext}$  ( $b_{ext\_CM}$ ). Regions are arranged from western to eastern United States (AK = Alaska, HI = Hawaii, NW = Northwest, CA = California, SW = Southwest, Cen = Central, MiS = Midsouth, NE = Northeast, SE = Southeast, VIIS = Virgin Islands, and US = all sites). Statistically significant trends ( $p \leq 0.05$ ) are denoted with “\*”.

## 7.7 AEROSOL EXTINCTION COEFFICIENT TRENDS

Reconstructed  $b_{\text{ext\_aer}}$  includes extinction from the previous aerosol species discussed, as well as  $b_{\text{ext\_ss}}$ . Rayleigh scattering contributions are not included. Trends in  $b_{\text{ext\_aer}}$  are likely similar to trends in total aerosol mass but could differ due to hygroscopic effects of some species, and because species with lower mass scattering efficiencies will have less contributions to extinction relative to mass (e.g., CM and FD).

The spatial patterns in long-term annual mean  $b_{\text{ext\_aer}}$  trends are shown in Figure 7.7.1a. The strongest reductions occurred at sites in the eastern United States, southern California, and the Northwest. Of the 38 valid sites, 34 had statistically significant trends. Sites with weak and insignificant trends were in California, Nevada, and Wyoming. Trends in  $b_{\text{ext\_aer}}$  ranged from  $-6.38\% \text{ yr}^{-1}$  ( $p < 0.001$ ) at Dolly Sods WA, West Virginia (DOSO1), to  $-0.57\% \text{ yr}^{-1}$  ( $p = 0.02$ ) at Guadalupe NP, Texas (GUMO1). The strong reduction of  $b_{\text{ext\_aer}}$  at eastern sites was likely associated with sulfate reductions (Hand et al., 2020).

The differences in long-term trends at sites in the eastern and western United States were also observed for short-term trends in annual mean  $b_{\text{ext\_aer}}$ , with the strongest reductions in the eastern United States where  $b_{\text{ext\_AS}}$  also significantly declined (Figure 7.7.1b). Positive but insignificant trends occurred at sites in California, Oregon, Washington, northern Montana, and North Dakota. This spatial pattern was similar to  $b_{\text{ext\_POM}}$  trends, and  $b_{\text{ext\_aer}}$  trends were likely influenced by the impacts of biomass smoke, especially at sites in the western United States. Short-term significant  $b_{\text{ext\_aer}}$  trends ranged from  $-8.44\% \text{ yr}^{-1}$  ( $p < 0.001$ ) at Shining Rock WA, North Carolina (SHRO1), to  $-1.16\% \text{ yr}^{-1}$  ( $p = 0.011$ ) at Salt Creek, New Mexico (SACR1).

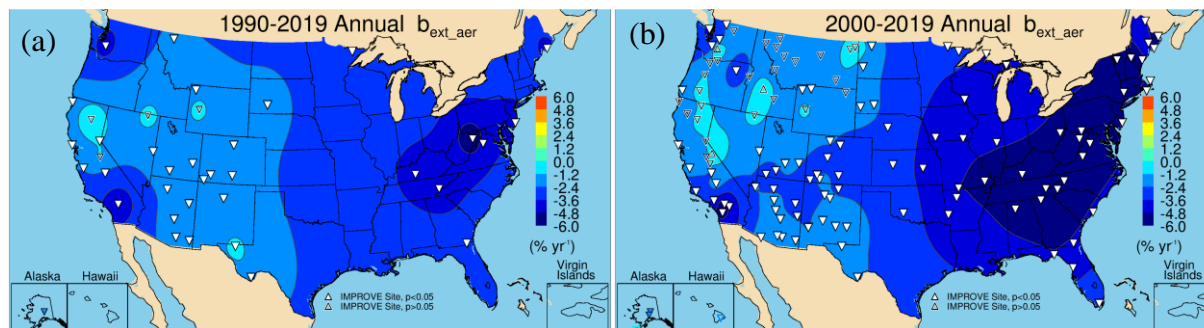


**Figure 7.7.1** Annual mean aerosol  $b_{\text{ext}}$  ( $b_{\text{ext\_aer}}$ ) trends ( $\% \text{ yr}^{-1}$ ) for (a) long-term (1990–2019) and (b) short-term (2000–2019) periods. Filled triangles correspond to statistically significant trends ( $p \leq 0.05$ ).

Comparisons of short-term regional and seasonal trends in  $b_{\text{ext\_aer}}$  are shown in Figure 7.7.2. The strong reductions in  $b_{\text{ext\_aer}}$  in eastern regions are similar to those for  $b_{\text{ext\_AS}}$  (Figure 7.1.2), suggesting that in the Northeast and Southeast regions,  $b_{\text{ext\_aer}}$  trends were largely driven by  $b_{\text{ext\_AS}}$ . The strongest regional reductions occurred during summer in the Northeast ( $-7.85\% \text{ yr}^{-1}$ ) and summer/fall in the Southeast region ( $-6.7\% \text{ yr}^{-1}$ ). While still negative, the magnitude of the trends decreased for western regions, around  $-2\% \text{ yr}^{-1}$  to  $-3\% \text{ yr}^{-1}$ . Regional trends in the western regions were influenced by biomass smoke, as indicated by the weak but insignificant trends during summer at sites in the Northwest and California regions, similar to  $b_{\text{ext\_POM}}$  (Figure 7.3.2). In addition,  $b_{\text{ext\_AS}}$  was lower in the western regions and did not decline at the same rate as in eastern regions (Hand et al., 2020).

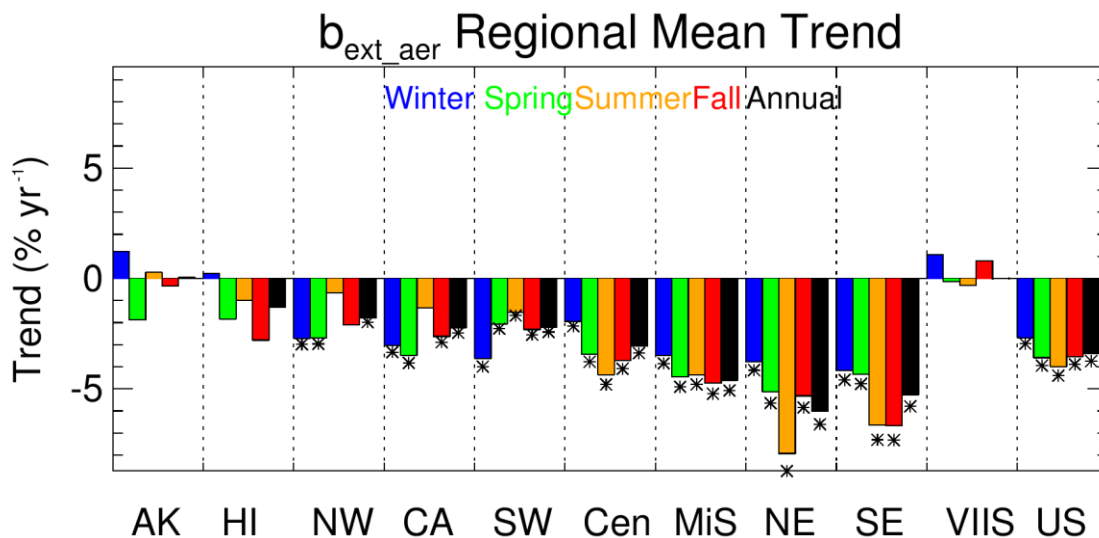


Figure 7.7.2. Short-term (2000–2019) regional seasonal mean aerosol  $b_{\text{ext}}$  ( $b_{\text{ext\_aer}}$ ) trends ( $\% \text{yr}^{-1}$ ) for major U.S. regions for winter, spring, summer, fall, and annual means. Regions are arranged from western to eastern United States (AK = Alaska, HI = Hawaii, NW = Northwest, CA = California, SW = Southwest, Cen = Central, MiS = Midsouth, NE = Northeast, SE = Southeast, VIIS = Virgin Islands, and US = all sites). Statistically significant trends ( $p \leq 0.05$ ) are denoted with “\*”.

The long-term 10<sup>th</sup> percentile trends in  $b_{\text{ext\_aer}}$  are shown in Figure 7.7.3a. All of the 40 valid trends were statistically significant. The strongest reductions occurred at sites in the Intermountain West, southern California, and the Appalachian Mountains. Trends ranged from  $-5.12\% \text{ yr}^{-1}$  ( $p < 0.001$ ) at Dolly Sods WA, West Virginia (DOSO1), to  $-1.80\% \text{ yr}^{-1}$  ( $p < 0.001$ ) at Pinnacles NM, California (PINN1). The 90<sup>th</sup> percentile trends in  $b_{\text{ext\_aer}}$  are shown in Figure 7.7.3b. Strong reductions in the eastern United States were likely associated with reductions in  $b_{\text{ext\_AS}}$ . Several sites in the West had insignificant trends, especially in California, Oregon, Nevada, Wyoming, and Texas. Trends ranged from  $-6.54\% \text{ yr}^{-1}$  ( $p < 0.001$ ) at DOSO1 to  $-0.89\% \text{ yr}^{-1}$  ( $p = 0.009$ ) at Bryce Canyon NP, Utah (BRCA1).

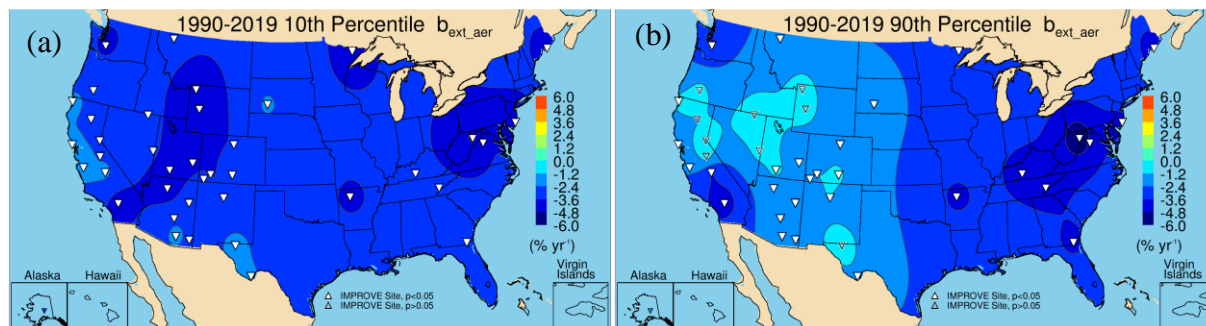
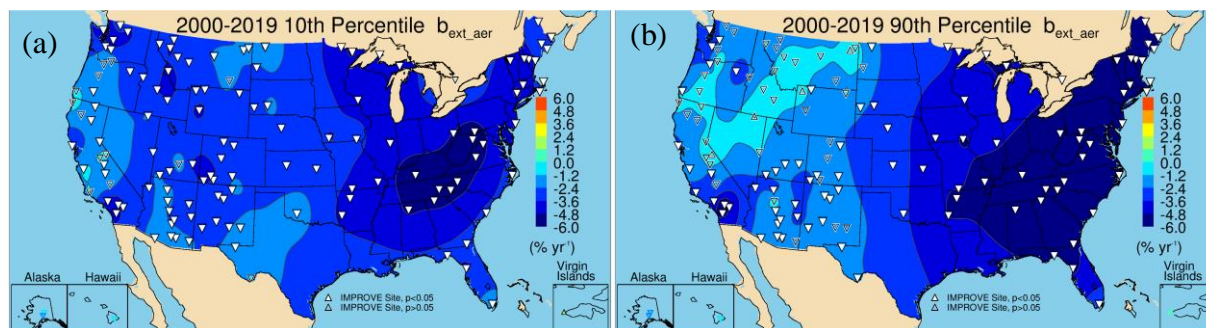


Figure 7.7.3. IMPROVE long-term (1990–2019) trends ( $\% \text{ yr}^{-1}$ ) in (a) 10<sup>th</sup> percentile aerosol  $b_{\text{ext}}$  ( $b_{\text{ext\_aer}}$ ) and (b) 90<sup>th</sup> percentile  $b_{\text{ext\_aer}}$ . Filled triangles correspond to statistically significant trends ( $p \leq 0.05$ ).

The short-term trends in 10<sup>th</sup> percentile  $b_{\text{ext\_aer}}$  were significant at 118 of the 136 valid sites (Figure 7.7.4a), with the strongest negative trends at sites in the eastern United States. Weaker trends occurred at sites in California and Oregon and in the northern Great Plains.

Trends ranged from  $-6.18\% \text{ yr}^{-1}$  ( $p < 0.001$ ) at Dolly Sods WA, West Virginia (DOSO1), to  $1.57\% \text{ yr}^{-1}$  ( $p = 0.03$ ) at Virgin Islands NP (VIIS1).

The spatial patterns in the short-term 90<sup>th</sup> percentile  $b_{\text{ext\_aer}}$  trends were similar to the long-term 90<sup>th</sup> percentiles trends (Figure 7.7.4b), with the strongest reductions at sites in the eastern United States. Of the 136 valid trends, 90 were statistically significant. Most of the insignificant trends occurred at sites in the West, likely influenced by biomass smoke. Trends ranged from  $-9.33\% \text{ yr}^{-1}$  at Cohutta, Georgia (COHU1), to  $-1.29\% \text{ yr}^{-1}$  ( $p = 0.03$ ) at Bandelier NM, New Mexico (BAND1).



**Figure 7.7.4. IMPROVE short-term (2000–2019) trends ( $\% \text{ yr}^{-1}$ ) in (a) 10<sup>th</sup> percentile aerosol  $b_{\text{ext}}$  ( $b_{\text{ext\_aer}}$ ) and (b) 90<sup>th</sup> percentile  $b_{\text{ext\_aer}}$ . Filled triangles correspond to statistically significant trends ( $p \leq 0.05$ ).**

The strongest regional mean short-term trends in  $b_{\text{ext\_aer}}$  occurred for the 90<sup>th</sup> percentile in the Northeast and Southeast regions ( $\sim -6.5\% \text{ yr}^{-1}$ ) and likely coincided with the strong summer mean  $b_{\text{ext\_aer}}$  trends (Figure 7.7.5). These trends are also consistent with strong reductions in summer mean  $b_{\text{ext\_AS}}$  in those regions. Trends in  $b_{\text{ext\_aer}}$  percentiles were weaker for regions in the West. The 10<sup>th</sup> and 50<sup>th</sup> percentile trends were the strongest in the Northwest and California regions, and the 90<sup>th</sup> percentile trends were likely associated with smoke influence. The Southwest region was the only western region with significant 90<sup>th</sup> percentile trends.

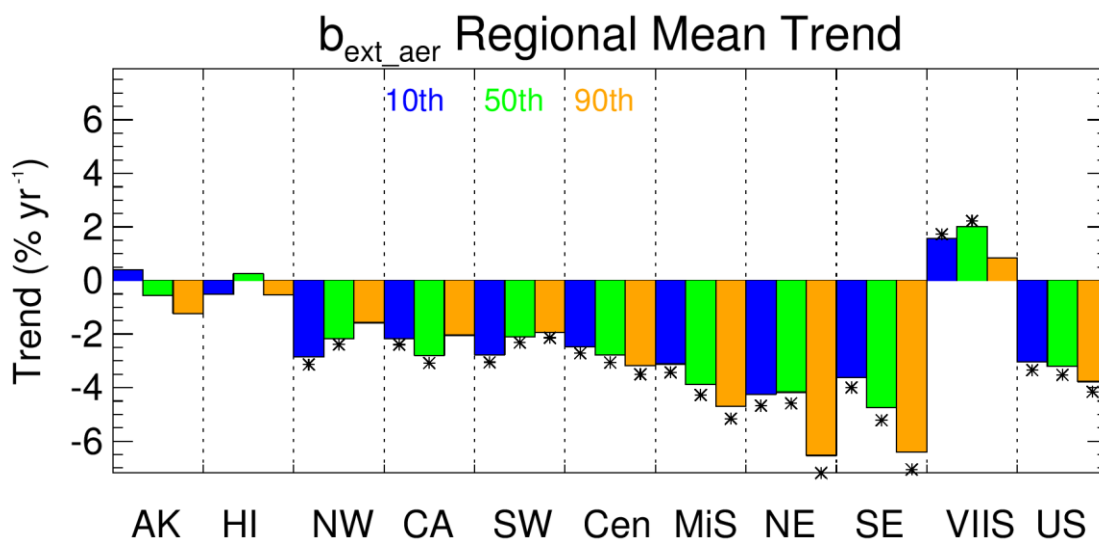


Figure 7.7.5. Short-term (2000–2019) regional mean trends ( $\% \text{ yr}^{-1}$ ) in 10<sup>th</sup>, 50<sup>th</sup>, and 90<sup>th</sup> percentile aerosol  $b_{\text{ext}}$  ( $b_{\text{ext\_aer}}$ ). Regions are arranged from western to eastern United States (AK = Alaska, HI = Hawaii, NW = Northwest, CA = California, SW = Southwest, Cen = Central, MiS = Midsouth, NE = Northeast, SE = Southeast, VIIS = Virgin Islands, and US = all sites). Statistically significant trends ( $p \leq 0.05$ ) are denoted with “\*”.

## 7.8 TOTAL EXTINCTION COEFFICIENT TRENDS

Reconstructed  $b_{\text{ext\_tot}}$  includes  $b_{\text{ext\_aer}}$  and site-specific Rayleigh scattering. Although the slopes from the linear regression will be the same for  $b_{\text{ext\_aer}}$  and  $b_{\text{ext\_tot}}$ , the trends in  $b_{\text{ext\_tot}}$  may be different because the normalization differs. However, general patterns in  $b_{\text{ext\_tot}}$  trends will follow trends in  $b_{\text{ext\_aer}}$ .

The spatial patterns in long-term annual mean  $b_{\text{ext\_tot}}$  trends are shown in (Figure 7.8.1a). The strongest reductions occurred at sites in the eastern United States, southern California, and the Northwest. Of the 38 valid sites, 34 had statistically significant trends. Sites with weaker and insignificant trends occurred in California, Nevada, and Wyoming. Trends in  $b_{\text{ext\_tot}}$  ranged from  $-6.38\% \text{ yr}^{-1}$  ( $p < 0.001$ ) at Dolly Sods WA, West Virginia (DOSO1), to  $-0.79\% \text{ yr}^{-1}$  ( $p = 0.02$ ) at Guadalupe NP, Texas (GUMO1). The strong reduction of  $b_{\text{ext\_tot}}$  at eastern sites was likely associated with sulfate reductions (Hand et al., 2020).

Similar spatial patterns occurred for short-term trends in annual mean  $b_{\text{ext\_tot}}$ , with the strongest reductions at sites in the eastern United States where  $b_{\text{ext\_AS}}$  significantly declined (Figure 7.8.1b). Positive but insignificant trends occurred at sites in California, Oregon, Washington, northern Montana, and North Dakota. This spatial pattern was similar to  $b_{\text{ext\_POM}}$  trends, and  $b_{\text{ext\_tot}}$  trends were likely influenced by the impacts of biomass smoke, especially at sites in the western United States. Short-term significant  $b_{\text{ext\_tot}}$  trends ranged from  $-6.53\% \text{ yr}^{-1}$  ( $p < 0.001$ ) at Shining Rock WA, North Carolina (SHRO1), to  $-0.71\% \text{ yr}^{-1}$  ( $p = 0.04$ ) at Trapper Creek, Alaska (TRCR1).

(b)

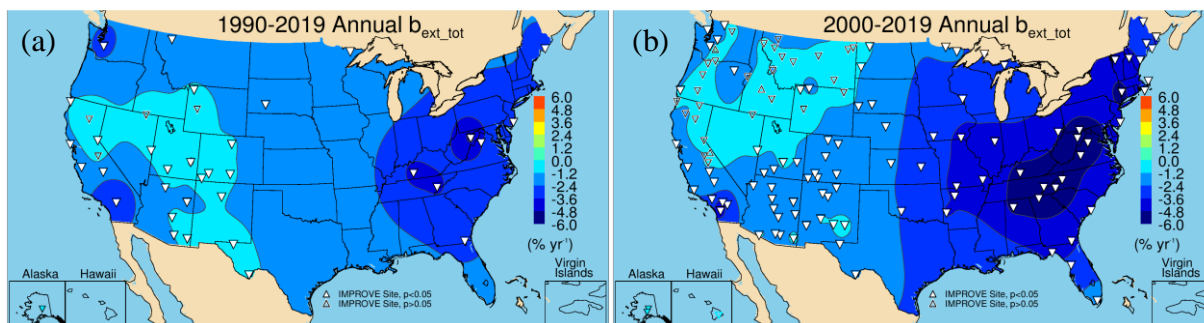


**Figure 7.8.1. Annual mean total  $b_{ext}$  ( $b_{ext\_tot}$ ) trends ( $\% \text{ yr}^{-1}$ ) for (a) long-term (1990–2019) and (b) short-term (2000–2019) periods. Filled triangles correspond to statistically significant trends ( $p \leq 0.05$ ).**

Comparisons of short-term regional and seasonal trends in  $b_{ext\_tot}$  are shown in Figure 7.8.2. The strong reductions in  $b_{ext\_tot}$  in eastern regions are similar to those for  $b_{ext\_AS}$  (Figure 7.1.2), suggesting that in the Northeast and Southeast regions,  $b_{ext\_tot}$  trends are largely driven by  $b_{ext\_AS}$ . The strongest regional reductions occurred during summer in the Northeast region ( $-6.51\% \text{ yr}^{-1}$ ) and summer/fall in the Southeast region ( $\sim -5.5\% \text{ yr}^{-1}$ ). While still negative, the magnitude of the trends decreased for western regions, around  $-2\% \text{ yr}^{-1}$  to  $-3\% \text{ yr}^{-1}$ . Regional trends in the western regions were influenced by biomass smoke, as evidenced by the weak but insignificant trends during summer in the Northwest and California regions, similar to  $b_{ext\_POM}$  (Figure 7.3.2). In addition,  $b_{ext\_AS}$  was lower in the western regions and did not decline at the same rate as in eastern regions.

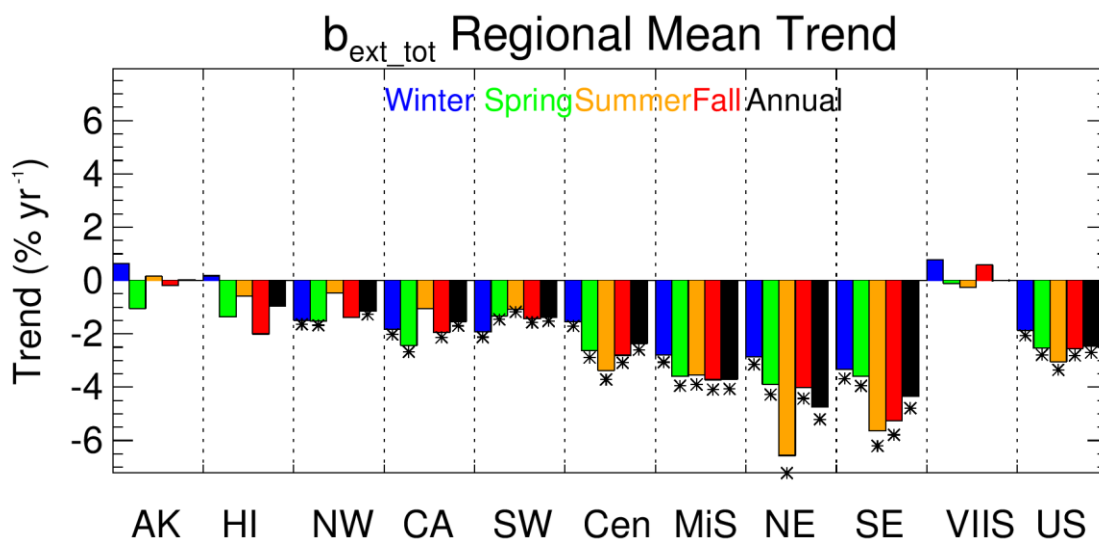


**Figure 7.8.2. Short-term (2000–2019) regional seasonal mean total  $b_{ext}$  ( $b_{ext\_tot}$ ) trends ( $\% \text{ yr}^{-1}$ ) for major U.S. regions for winter, spring, summer, fall, and annual means. Regions are arranged from western to eastern United States (AK = Alaska, HI = Hawaii, NW = Northwest, CA = California, SW = Southwest, Cen = Central, MiS = Midsouth, NE = Northeast, SE = Southeast, VIIS = Virgin Islands, and US = all sites). Statistically significant trends ( $p \leq 0.05$ ) are denoted with “\*”.**

The long-term 10<sup>th</sup> percentile trends in  $b_{ext\_tot}$  are shown in Figure 7.8.3a. All of the 40 valid trends were statistically significant. The strongest reductions occurred at sites in the

Intermountain West, southern California, and the Appalachian Mountains. Trends ranged from  $-3.39\% \text{ yr}^{-1}$  ( $p < 0.001$ ) at Dolly Sods WA, West Virginia (DOSO1), to  $-0.65\% \text{ yr}^{-1}$  ( $p < 0.001$ ) at Denali NP, Alaska (DENA1). The 90<sup>th</sup> percentile trends in  $b_{\text{ext\_tot}}$  are shown in Figure 7.8.3b. Strong reductions in the eastern United States were likely associated with reductions in  $b_{\text{ext\_AS}}$ . Several sites in the West had insignificant trends, especially at sites in California, Oregon, Nevada, Wyoming, and Texas. Trends ranged from  $-5.97\% \text{ yr}^{-1}$  ( $p < 0.001$ ) at DOSO1 to  $-0.63\% \text{ yr}^{-1}$  ( $p = 0.009$ ) at Bryce Canyon NP, Utah (BRCA1).

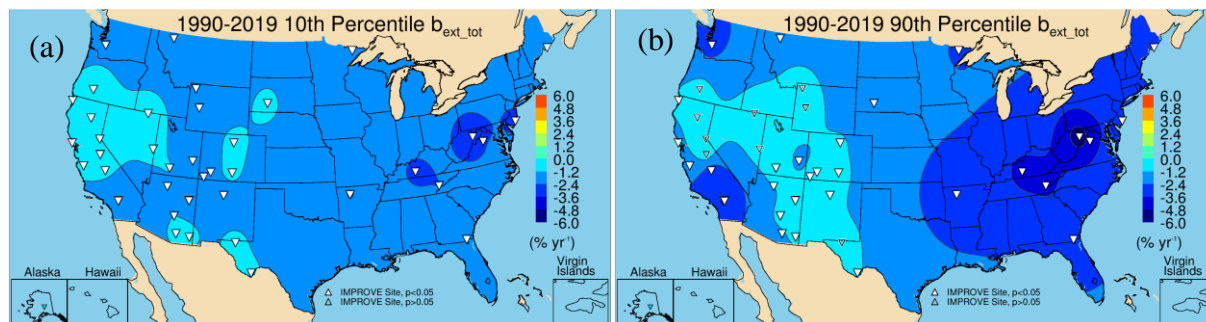


**Figure 7.8.3. IMPROVE long-term (1990–2019) trends ( $\% \text{ yr}^{-1}$ ) in (a) 10<sup>th</sup> percentile total  $b_{\text{ext}}$  ( $b_{\text{ext\_tot}}$ ) and (b) 90<sup>th</sup> percentile  $b_{\text{ext\_tot}}$ . Filled triangles correspond to statistically significant trends ( $p \leq 0.05$ ).**

The short-term trends in 10<sup>th</sup> percentile  $b_{\text{ext\_tot}}$  were significant at 118 of the 136 valid sites (Figure 7.8.4a), with the strongest negative trends at sites in the eastern United States. Weaker trends occurred at sites in California, Oregon, and the northern Great Plains. Trends ranged from  $-4.26\% \text{ yr}^{-1}$  ( $p < 0.001$ ) at Mammoth Cave NP, Kentucky (MACA1), to  $0.94\% \text{ yr}^{-1}$  ( $p = 0.03$ ) at Virgin Islands NP (VIIS1).

The spatial patterns in the short-term 90<sup>th</sup> percentile  $b_{\text{ext\_tot}}$  trends were similar to the long-term 90<sup>th</sup> percentiles trends (Figure 7.8.4b), with the strongest reductions at sites in the eastern United States. Of the 136 valid trends, 90 were statistically significant. Most of the insignificant trends occurred at sites in the West, likely influenced by biomass smoke. Trends ranged from  $-8.28\% \text{ yr}^{-1}$  at Cohutta, Georgia (COHU1), to  $-0.93\% \text{ yr}^{-1}$  ( $p = 0.03$ ) at Bandelier NM, New Mexico (BAND1).

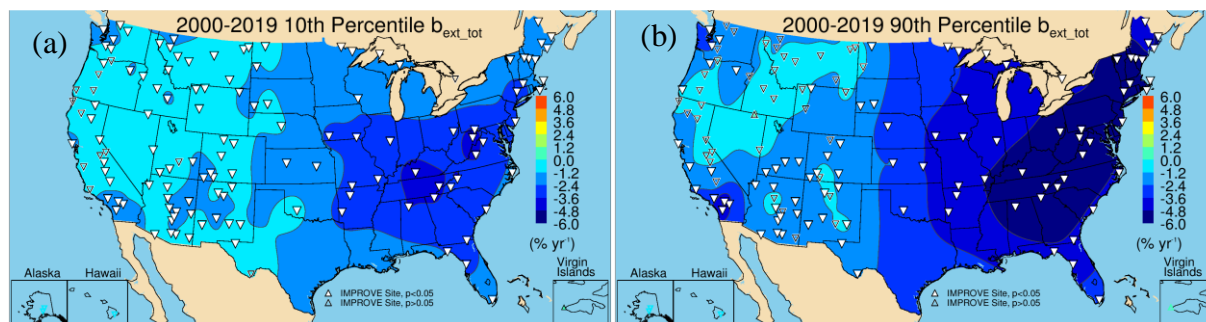


**Figure 7.8.4. IMPROVE short-term (2000–2019) trends ( $\% \text{ yr}^{-1}$ ) in (a) 10<sup>th</sup> percentile total  $b_{\text{ext}}$  ( $b_{\text{ext\_tot}}$ ) and (b) 90<sup>th</sup> percentile  $b_{\text{ext\_tot}}$ . Filled triangles correspond to statistically significant trends ( $p \leq 0.05$ ).**

The strongest regional mean short-term trends in  $b_{\text{ext\_tot}}$  occurred for the 90<sup>th</sup> percentile in the Northeast and Southeast regions ( $\sim -5.5\% \text{ yr}^{-1}$ ) and coincided with the strong summer mean

$b_{\text{ext\_tot}}$  trends (Figure 7.8.5). These trends were consistent with strong reductions in summer mean  $b_{\text{ext\_AS}}$  in those regions. Trends in  $b_{\text{ext\_tot}}$  percentiles were weaker for regions in the West. The 10<sup>th</sup> and 50<sup>th</sup> percentile trends were the strongest in the Northwest and California regions, and insignificant 90<sup>th</sup> percentile trends were likely associated with smoke influence. The Southwest region was the only western region with significant 90<sup>th</sup> percentile trends.

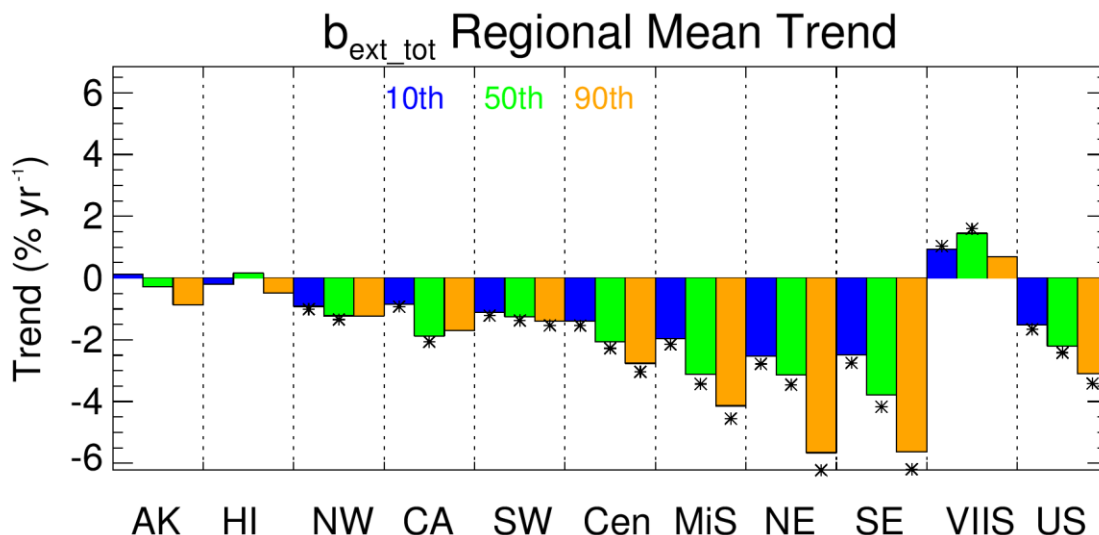


**Figure 7.8.5. Short-term (2000–2019) regional mean trends (% yr<sup>-1</sup>) in 10<sup>th</sup>, 50<sup>th</sup>, and 90<sup>th</sup> percentile total  $b_{\text{ext}}$  ( $b_{\text{ext\_tot}}$ ). Regions are arranged from western to eastern United States (AK = Alaska, HI = Hawaii, NW = Northwest, CA= California, SW = Southwest, Cen = Central, MiS = Midsouth, NE = Northeast, SE = Southeast, VIIS = Virgin Islands, and US = all sites). Statistically significant trends ( $p \leq 0.05$ ) are denoted with “\*”.**

## 7.9 DECIVIEW TRENDS

The deciview (dv) haze index is a logarithmic transformation of  $b_{\text{ext\_tot}}$  (see Chapter 4.1); therefore, the spatial and seasonal patterns in dv trends will generally follow trends in  $b_{\text{ext\_tot}}$ . The spatial patterns in long-term annual mean dv trends are shown in (Figure 7.9.1a). The strongest reductions occurred at sites in the eastern United States, southern California, and the Northwest. Of the 38 valid sites, 37 had statistically significant trends. Sites with lower and insignificant trends were in California, Nevada, and Wyoming. Trends in dv ranged from  $-2.85\% \text{ yr}^{-1}$  ( $p < 0.001$ ) at Dolly Sods WA, West Virginia (DOS01), to  $-0.53\% \text{ yr}^{-1}$  ( $p = 0.009$ ) at Guadalupe NP, Texas (GUMO1).

The differences in annual mean dv trends that were observed between sites in the eastern and western United States were also observed for the short-term trends, with the strongest reductions in the eastern United States where  $b_{\text{ext\_AS}}$  significantly declined (Figure 7.9.1b). Insignificant trends occurred at sites in California, Oregon, Washington, northern Montana, and North Dakota. This spatial pattern was similar to  $b_{\text{ext\_POM}}$  trends, and dv trends were influenced by the impacts of biomass smoke, especially at sites in the western United States. Short-term significant dv trends ranged from  $-3.81\% \text{ yr}^{-1}$  ( $p < 0.001$ ) at Shining Rock WA, North Carolina (SHRO1), to  $-0.67\% \text{ yr}^{-1}$  ( $p = 0.013$ ) at Salt Creek, New Mexico (SACR1).

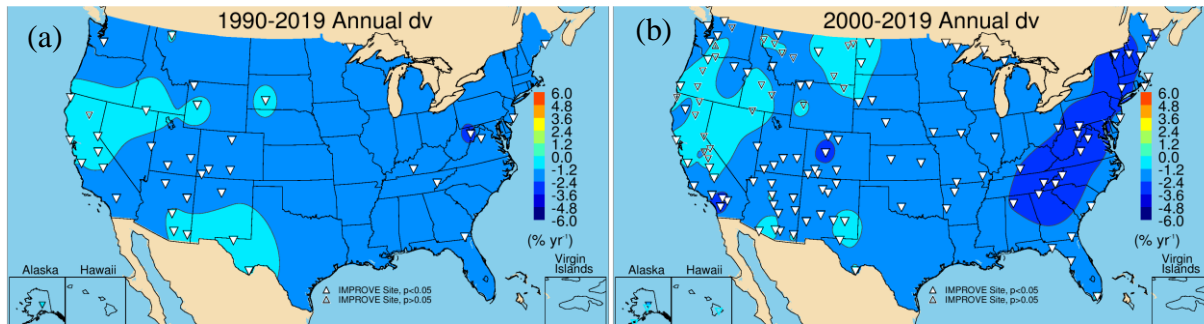


**Figure 7.9.1 Annual mean deciview (dv) trends (% yr<sup>-1</sup>) for (a) long-term (1990–2019) and (b) short-term (2000–2019) periods. Filled triangles correspond to statistically significant trends ( $p \leq 0.05$ ).**

Comparisons of short-term regional and seasonal mean trends in dv are shown in Figure 7.9.2. The strong reductions in dv in eastern regions are similar to those for  $b_{\text{ext\_AS}}$  (Figure 7.1.2), suggesting that in the Northeast and Southeast regions, dv trends were largely driven by  $b_{\text{ext\_AS}}$ . The strongest regional reductions occurred during summer in the Northeast region ( $-3.24\% \text{ yr}^{-1}$ ) and summer/fall in the Southeast region ( $\sim -2.7\% \text{ yr}^{-1}$ ). While still negative, the magnitude of the trends decreased for western regions, around  $-1\% \text{ yr}^{-1}$  to  $-2\% \text{ yr}^{-1}$ . Regional trends in the western regions were influenced by biomass smoke, as evidenced by the weak but insignificant trends during summer in the Northwest and California regions, similar to  $b_{\text{ext\_POM}}$  (Figure 7.3.2). In addition,  $b_{\text{ext\_AS}}$  was lower in the western regions and did not decline at the same rate as in eastern regions.

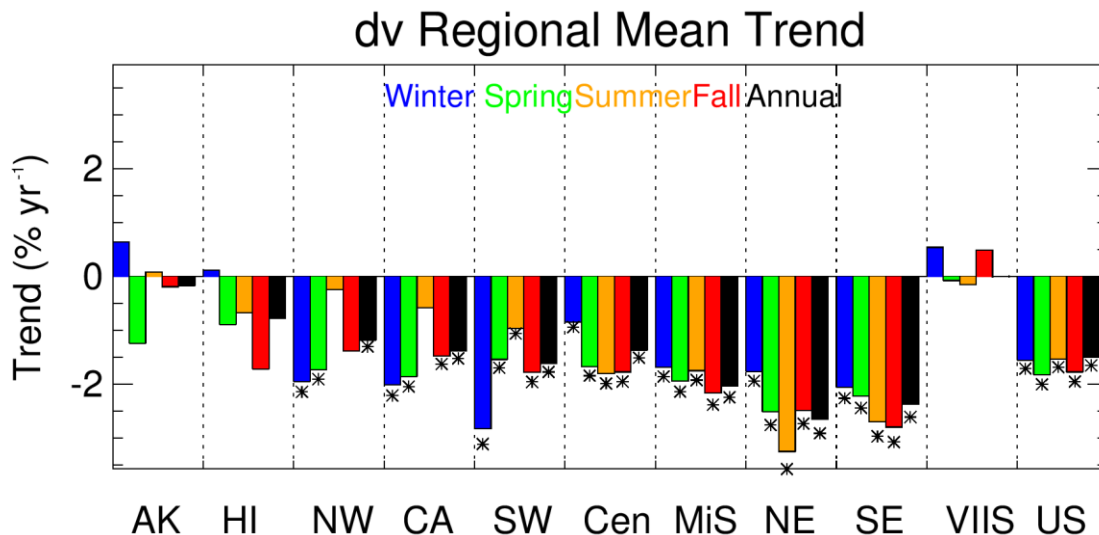


**Figure 7.9.2. Short-term (2000–2019) regional seasonal mean deciview (dv) trends (% yr<sup>-1</sup>) for major U.S. regions for winter, spring, summer, fall, and annual means. Regions are arranged from western to eastern United States (AK = Alaska, HI = Hawaii, NW = Northwest, CA = California, SW = Southwest, Cen = Central, MiS = Midsouth, NE = Northeast, SE = Southeast, VIIS = Virgin Islands, and US = all sites). Statistically significant trends ( $p \leq 0.05$ ) are denoted with “\*”.**

The long-term 10<sup>th</sup> percentile trends in dv are shown in Figure 7.9.3a. All of the 40 valid trends were statistically significant. The strongest reductions occurred at sites in the

Intermountain West, southern California, and the Appalachian Mountains. Trends ranged from  $-6.32\% \text{ yr}^{-1}$  ( $p < 0.001$ ) at Bridger, Wyoming (BRID1), to  $-1.08\% \text{ yr}^{-1}$  ( $p < 0.001$ ) at Pinnacles NM, California (PINN1). The 90<sup>th</sup> percentile long-term trends in  $dv$  are shown in Figure 7.9.3b. Strong reductions in the eastern United States were likely associated with reductions in  $b_{\text{ext\_AS}}$ . Several sites in the West had insignificant trends, especially at sites in California, Oregon, Nevada, Wyoming, and Texas. Trends ranged from  $-2.41\% \text{ yr}^{-1}$  ( $p < 0.001$ ) at Dolly Sods WA, West Virginia (DOSO1), to  $-0.41\% \text{ yr}^{-1}$  ( $p = 0.03$ ) at Redwood NP, California (REDW1).

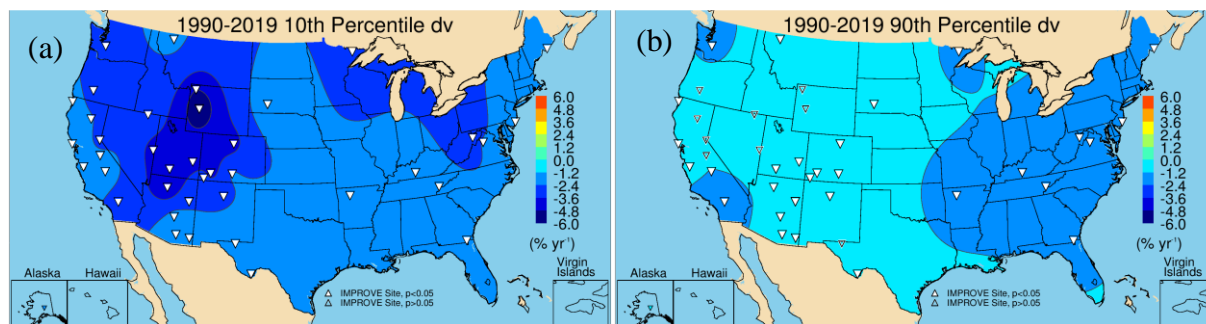


**Figure 7.9.3. IMPROVE long-term (1990–2019) trends ( $\% \text{ yr}^{-1}$ ) in (a) 10<sup>th</sup> percentile deciview ( $dv$ ) and (b) 90<sup>th</sup> percentile  $dv$ . Filled triangles correspond to statistically significant trends ( $p \leq 0.05$ ).**

The short-term trends in 10<sup>th</sup> percentile  $dv$  were significant at 118 of the 136 valid sites (Figure 7.9.4a), with the strongest negative trends at sites in the eastern United States. Weaker trends occurred at sites in California, Oregon, and the northern Great Plains. Trends ranged from  $-9.42\% \text{ yr}^{-1}$  ( $p < 0.001$ ) at White River NF, Colorado (WHR11), to  $0.92\% \text{ yr}^{-1}$  ( $p = 0.03$ ) at Virgin Islands NP (VIIS1).

The spatial pattern in the short-term 90<sup>th</sup> percentile  $dv$  trends (Figure 7.9.4b) showed the strongest reductions at sites in the eastern United States. Of the 136 valid trends, 90 were statistically significant. Most of the insignificant trends occurred at sites in the West, likely influenced by biomass smoke. Trends ranged from  $-3.47\% \text{ yr}^{-1}$  ( $p < 0.001$ ) at Shining Rock WA, North Carolina (SHRO1), to  $-0.74\% \text{ yr}^{-1}$  ( $p = 0.03$ ) at Kalmiopsis, Oregon (KALM1).

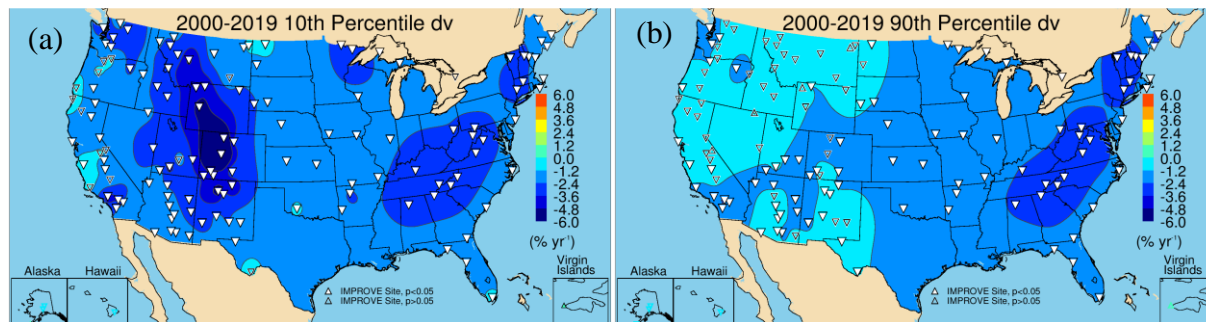


**Figure 7.9.4. IMPROVE short-term (2000–2019) trends ( $\% \text{ yr}^{-1}$ ) in (a) 10<sup>th</sup> percentile deciview ( $dv$ ) and (b) 90<sup>th</sup> percentile  $dv$ . Filled triangles correspond to statistically significant trends ( $p \leq 0.05$ ).**

The strongest regional short-term trends in  $dv$  occurred for the 90<sup>th</sup> percentile in the Northeast and Southeast regions ( $\sim -2.5\% \text{ yr}^{-1}$ ) and likely coincided with the strong summer mean

dv trends (Figure 7.9.5). These trends were consistent with strong reductions in summer mean  $b_{ext\_AS}$  in those regions. Trends in dv percentiles decreased for regions in the West. The 10<sup>th</sup> and 50<sup>th</sup> percentile trends were the strongest in the Northwest and California regions, and insignificant 90<sup>th</sup> percentile trends were likely associated with smoke influence. The Southwest region was the only western region with significant 90<sup>th</sup> percentile trends.

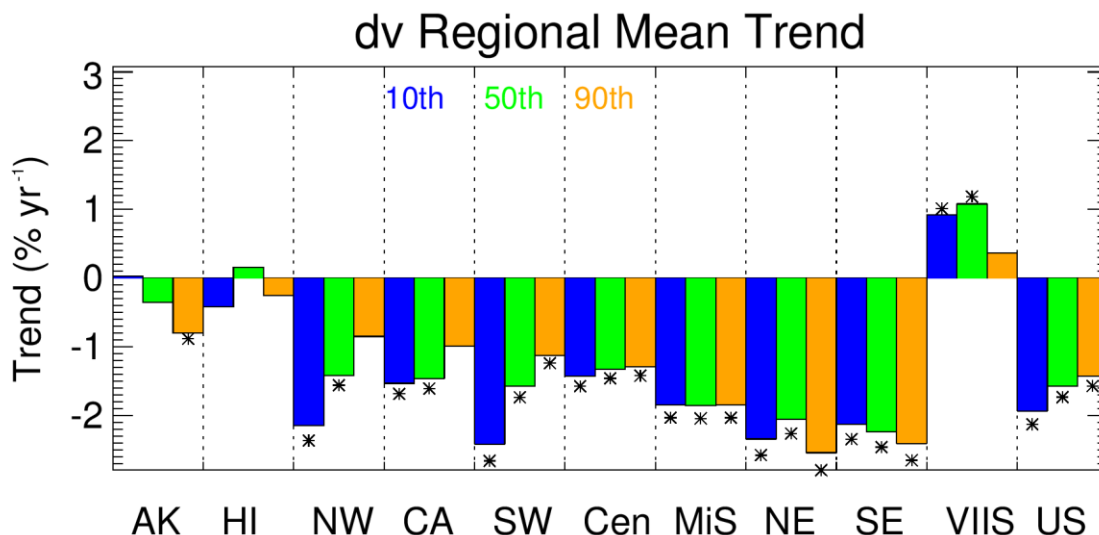


**Figure 7.9.5.** Short-term (2000–2019) trends (% yr<sup>-1</sup>) trends in 10<sup>th</sup>, 50<sup>th</sup>, and 90<sup>th</sup> percentile deciview (dv). Regions are arranged from western to eastern United States (AK = Alaska, HI = Hawaii, NW = Northwest, CA= California, SW = Southwest, Cen = Central, MiS = Midsouth, NE = Northeast, SE = Southeast, VIIS = Virgin Islands, and US = all sites). Statistically significant trends ( $p \leq 0.05$ ) are denoted with “\*”.

## 7.10 DISCUSSION

Timelines of regional, annual mean speciated  $b_{ext}$  corresponding to the previous trend results are shown in Figure 7.10.1(a-j) for 2000 through 2019 due to the expansion of the network in 2000 (Hand et al., 2020). Strong reductions in  $b_{ext\_tot}$  have occurred at remote sites across the United States. These reductions were greatest in the eastern United States and driven by strong negative trends in  $b_{ext\_AS}$ . Sulfate concentrations and associated  $b_{ext\_AS}$  have decreased in response to major reductions in sulfur dioxide emissions (Hand et al., 2020). In addition, reductions in  $b_{ext\_AN}$  and  $b_{ext\_POM}$  (especially in the East) have contributed to reduced  $b_{ext\_tot}$ . Negative trends in  $b_{ext\_tot}$  occurred at sites in California where  $b_{ext\_AN}$  decreased due to reductions in nitrogen dioxide emissions, especially mobile emissions.

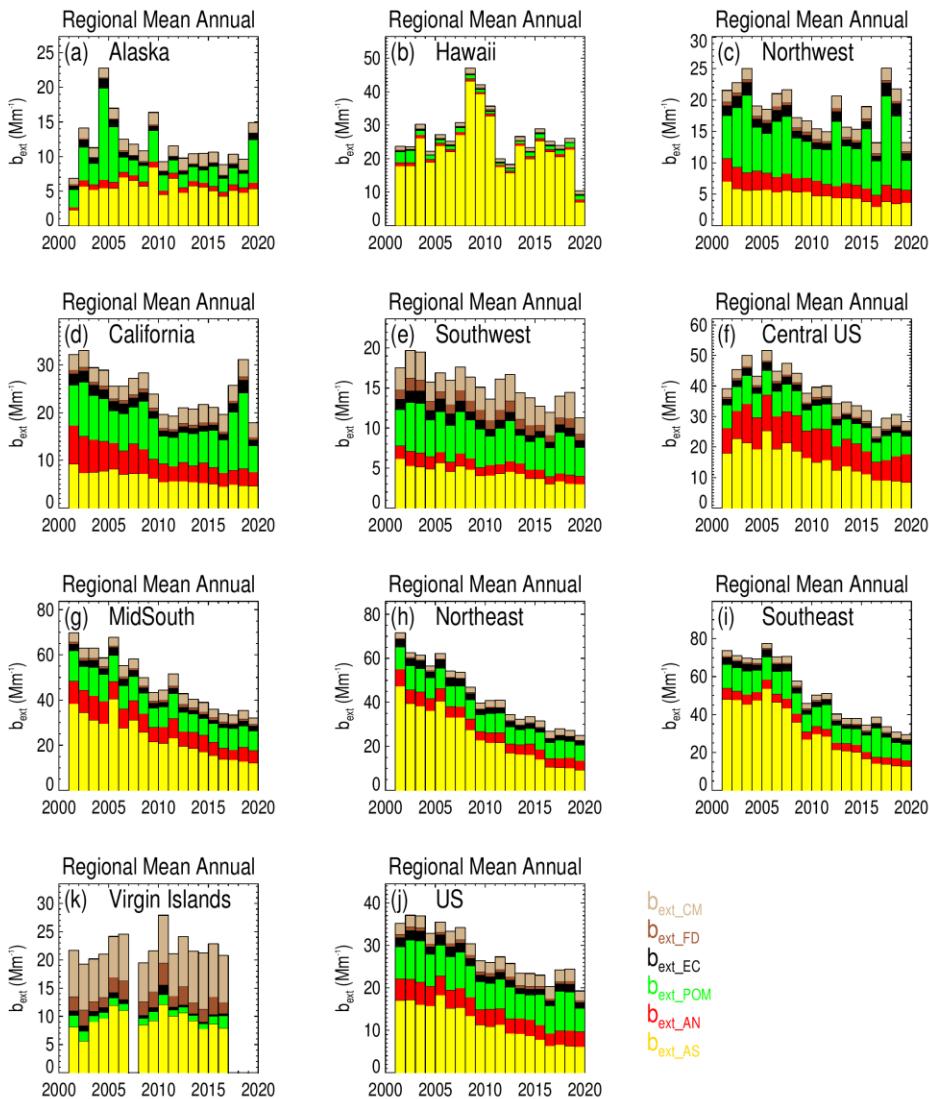


**Figure 7.10.1. Short-term (2001–2019) timelines in IMPROVE regional, annual mean ambient speciated  $b_{ext}$  ( $Mm^{-1}$ ) for ammonium sulfate ( $b_{ext\_AS}$ ), ammonium nitrate ( $b_{ext\_AN}$ ), particulate organic matter ( $b_{ext\_POM}$ ), elemental carbon ( $b_{ext\_EC}$ ), fine dust ( $b_{ext\_FD}$ ), and coarse mass ( $b_{ext\_CM}$ ). Wavelength corresponds to 550 nm.**

In the western United States, especially the Northwest,  $b_{ext\_tot}$  has declined at a weaker rate relative to sites in the East. Comparisons of  $b_{ext\_POM}$  and  $b_{ext\_EC}$  trends suggest that  $b_{ext\_tot}$  is influenced by an increase in biomass burning impacts that have led to an increase in  $b_{ext\_POM}$ , or at the very least flat and insignificant trends (Figure 7.10.1c). Extinction from carbonaceous aerosols is a major contributor to  $b_{ext\_tot}$  especially at western sites (Hand et al., 2020).

Although  $b_{ext\_FD}$  and  $b_{ext\_CM}$  have not decreased at the same rate as extinction from other species, and in some regions have increased, their impact on  $b_{ext\_tot}$  was not as pronounced as their impact on mass. This difference is due to their lower mass scattering efficiencies (compare Figure 7.10.1 to Figures 6.10.1 and 6.10.2). However, the fraction of  $b_{ext\_tot}$  due to  $b_{ext\_FD}$  and  $b_{ext\_CM}$  has increased, especially as  $b_{ext\_AS}$  and  $b_{ext\_AN}$  have decreased.

Regulatory activity has been very successful at reducing pollutant emissions that lead to secondary aerosols, such as sulfate, nitrate, and POM, and their contributions to haze. Reductions in these species have driven negative trends in  $b_{\text{ext\_tot}}$  at sites across the United States. However, the role of natural aerosols, such as those derived from biomass smoke and dust storms, have not declined and for some sites and seasons, have increased. The impacts of these positive trends have and likely will continue to impede progress in improving visibility, especially in the western United States.

To demonstrate the visibility conditions associated with the trends in  $b_{\text{ext\_tot}}$ , the computer software program, WinHaze 2.9.9.1 (<http://vista.cira.colostate/Improve/win haze>) was used to simulate visibility conditions from user-specified scenes and speciated aerosol concentrations or visibility levels. The 90<sup>th</sup> percentile  $b_{\text{ext\_tot}}$  values were chosen for the initial and end years for Great Smoky Mountains NP, Tennessee (GRSM1), San Geronio WA, California (SAGO1), and Yosemite NP, California (YOSE1). These sites were chosen to represent trends in visibility in the East and West, respectively.

The 90<sup>th</sup> percentile visibility conditions in GRSM1 in 1990 ( $256 \text{ Mm}^{-1}$ ) and 2019 ( $58 \text{ Mm}^{-1}$ ) are shown in Figure 7.10.2. The dramatic improvement in the visibility conditions is evident. These changes are largely due to the reductions of sulfate aerosols in the region and were evidenced by the strong reduction in  $b_{\text{ext\_tot}}$  shown in Figure 7.8.4b. Similar results for the 1990 ( $127 \text{ Mm}^{-1}$ ) and 2019 ( $43 \text{ Mm}^{-1}$ ) 90<sup>th</sup> percentile  $b_{\text{ext\_tot}}$  at SAGO1 are shown in Figure 7.10.3. The striking improvement in visibility at this site was largely due to the reduction of nitrate aerosols. In contrast, visibility conditions at Yosemite NP, California, are shown in Figure 7.10.4 for the 90<sup>th</sup> percentile  $b_{\text{ext\_tot}}$  in 1990 ( $58 \text{ Mm}^{-1}$ ) and 2019 ( $40 \text{ Mm}^{-1}$ ). The changes in the conditions are imperceptible, in part because the initial conditions were initially very low. This site had insignificant trends and was influenced by biomass smoke impacts. While the trend analyses presented here provide a quantifiable measure of the changes in haze over time, the ability to visualize the changes is a powerful means by which to communicate the progress that has been achieved through regulatory activity, as well as to identify future challenges.

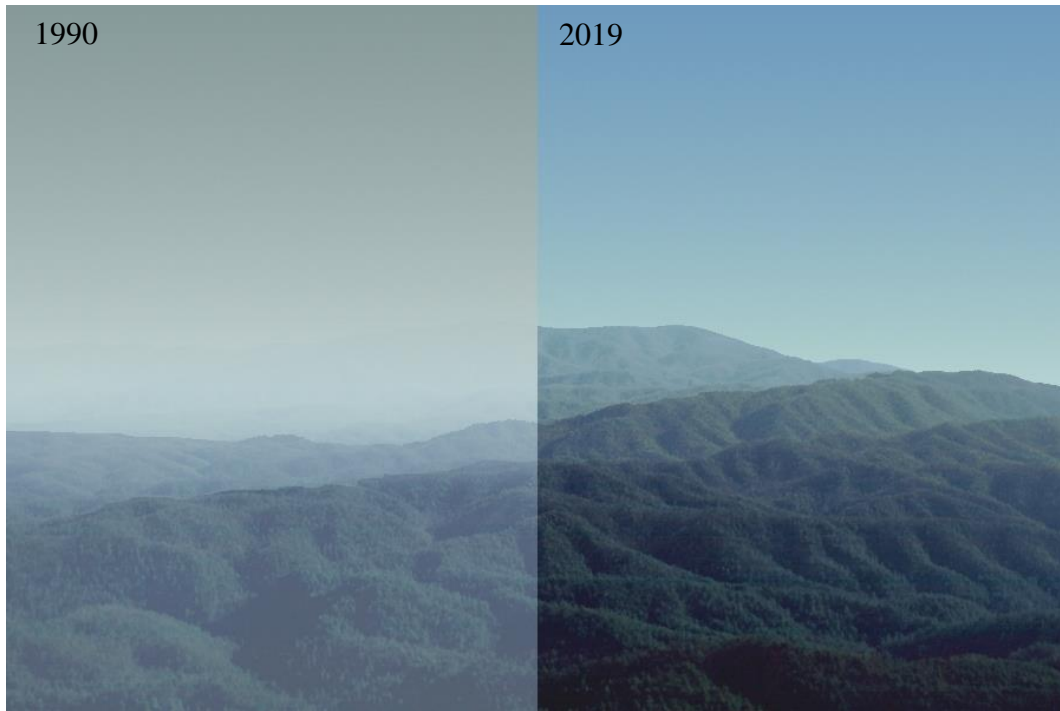


**Figure 7.10.2. Split-image of visibility conditions in Great Smoky Mountains NP, Tennessee (GRSM1), for 90<sup>th</sup> percentile total extinction levels in 1990 (left side) and 2019 (right side).**

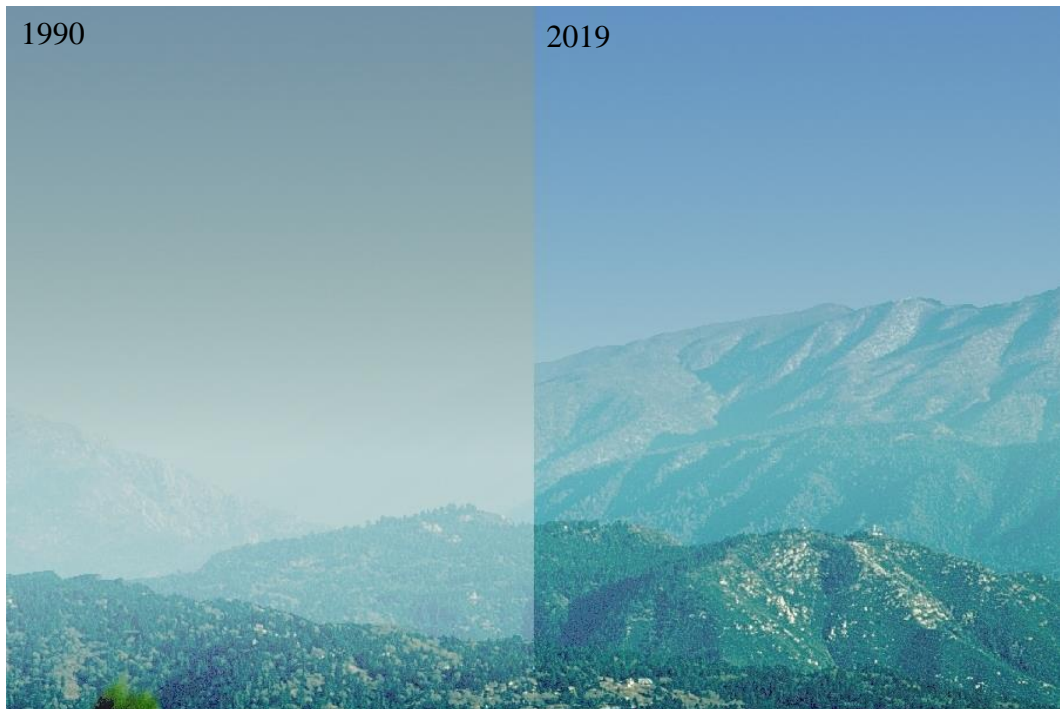


**Figure 7.10.3. Split-image of visibility conditions in San Gorgonio WA, California (SAGO1), for 90<sup>th</sup> percentile total extinction levels in 1990 (left side) and 2019 (right side).**



**Figure 7.10.4. Split-image of visibility conditions in Yosemite NP, California (YOSE1), for 90<sup>th</sup> percentile total extinction levels in 1990 (left side) and 2019 (right side).**

Site-specific long-term and short-term trend results are provided in Appendix 7.1 for annual mean trends, short-term percentile trends in Appendix 7.2, and long-term percentile trends in Appendix 7.3.

## REFERENCES

- Gebhart, K. A., Day, D. E., Prenni, A. J., Schichtel, B. A., Hand, J. L., and Evanski-Cole, A. R. (2018), Visibility impacts at Class I areas near the Bakken oil and gas development, *Journal of the Air & Waste Management Association*, 68(5), 477-493, doi:10.1080/10962247.2018.1429334.
- Hand, J. L., Schichtel, B. A., Malm, W. C., and Pitchford, M. L. (2012), Particulate sulfate ion concentration and SO<sub>2</sub> emission trends in the United States from the early 1990s through 2010, *Atmospheric Chemistry and Physics*, 12(21), 10353-10365, doi:10.5194/acp-12-10353-2012.
- Hand, J. L., Schichtel, B. A., Malm, W. C., Copeland, S., Molenaar, J. V., Frank, N. H., and Pitchford, M. (2014), Widespread reductions in haze across the United States from the early 1990s through 2011, *Atmospheric Environment*, 94, 671-679, doi:10.1016/j.atmosenv.2014.05.062.
- Hand, J. L., Prenni, A. J., Copeland, S., Schichtel, B. A., and Malm, W. C. (2020), Thirty years of the Clean Air Act Amendments: Impacts on haze in remote regions of the United States (1990–2018), *Atmospheric Environment*, 243, 117865, <https://doi.org/10.1016/j.atmosenv.2020.117865>.
- Isaaks, E. H., and Mohan Srivastava, R. (1989), *An Introduction to Applied Geostatistics*, Oxford University Press, New York, ISBN 978-0195050134.
- McClure, C. D., and Jaffe, D. A. (2018), US particulate matter air quality improves except in wildfire-prone areas, *Proceedings of the National Academy of Sciences*, 115(31), 7901-7906, doi:10.1073/pnas.1804353115.
- Russell, A., Valin, L., and Cohen, R. (2012), Trends in OMI NO<sub>2</sub> observations over the United States: Effects of emission control technology and the economic recession, *Atmospheric Chemistry and Physics*, 12(24), 12197-12209, doi:doi:10.5194/acp-12-12197-2012.
- Theil, H. (1950), A rank-invariant method of linear and polynomial regression analysis., *Proc. Kon. Ned. Akad. v Wetensch.*, A(53), 386-392, [https://doi.org/10.1007/978094-011-2546-8\\_20](https://doi.org/10.1007/978094-011-2546-8_20).
- Tong, D. Q., Lamsal, L., Pan, L., Ding, C., Kim, H., Lee, P., Chai, T., Pickering, K. E., and Stajner, I. (2015), Long-term NO<sub>x</sub> trends over large cities in the United States during the great recession: Comparison of satellite retrievals, ground observations, and emission inventories, *Atmospheric Environment*, 107, 70-84, <http://dx.doi.org/10.1016/j.atmosenv.2015.01.035>.
- Zhang, X. (2019), Correction of chloride concentrations for filter blank levels, *IMPROVE Data Advisory* (da0039), [http://vista.cira.colostate.edu/improve/Data/QA\\_QC/Advisory/da0039/da0039\\_ChlorideOverCorrection.pdf](http://vista.cira.colostate.edu/improve/Data/QA_QC/Advisory/da0039/da0039_ChlorideOverCorrection.pdf).